Marine Geology 491 (2026) 107660

Contents lists available at ScienceDirect

Marine Geology

journal homepage: www.elsevier.com/locate/margo

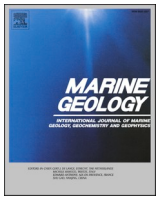

Research Article

The incompleteness of turbidite records: Comparing direct monitoring of turbidity currents to deposits preserved in submarine fans (Pointe-des-Monts, eastern Canada)

Florian Jacques [a,b,c,*], Alexandre Normandeau [d], Jean-Carlos Montero-Serrano [b,c,*], Guillaume St-Onge [a,c], Audrey Limoges [e], André Rochon [b,c], Urs Neumeier [b], Patrick Lajeunesse [f], Daniel Bourgault [b]

[a] Canada Research Chair in Marine Geology, Institut des sciences de la mer (ISMER), Université du Québec à Rimouski (UQAR), Québec-Océan, 310 All. des Ursulines, Rimouski, QC G5L 2Z9, Canada
[b] Institut des sciences de la mer (ISMER), Université du Québec à Rimouski (UQAR), Québec-Océan, 310 All. des Ursulines, Rimouski, QC G5L 2Z9, Canada
[c] Geotop Research Center, 201 Av. du Président-Kennedy, Montréal, QC H2X 3Y7, Canada
[d] Geological Survey of Canada (Atlantic), 1 Challenger Dr, Dartmouth, NS B2Y 4A2, Canada
[e] Department of Earth Sciences, University of New Brunswick, 2 Bailey Drive, Fredericton, NB E3B 5A3, Canada
[f] Département de Géographie, Université Laval, Pavillon Abitibi-Price, 2405 Rue de la Terrasse, Québec, QC G1V 0A6, Canada

ARTICLE INFO

Editor: Michele Rebesco

Keywords:
Turbidity currents
Bottom current remobilization
Acoustic Doppler current profiler
Repeat multibeam bathymetry
Sediment cores
Cyclic steps
St. Lawrence Estuary
Storms

ABSTRACT

The recurrence of turbidity currents in submarine canyons is often assessed using sediment core records from submarine fans, which are generally assumed to reflect canyon processes. However, this assumption has rarely been tested. Here, we assess the completeness of modern sedimentary records in the Pointe-des-Monts submarine fan, located in the Lower St. Lawrence Estuary, eastern Canada, by comparing turbidity current activity derived from repeat multibeam bathymetry, direct monitoring observations, and short sediment cores. The timelapse bathymetry and monitoring results revealed that turbidity current activity over the last 15 years was primarily driven by storms, especially during ice-free winters. Since 2007, a minimum of nine turbidity currents were recorded by timelapse multibeam bathymetry and direct observations in the canyon system, many of which have led to the migration of cyclic steps within the canyon axis. However, turbidites recorded in the short sediment cores on the lobe predate all monitoring efforts, indicating a largely incomplete record of canyon processes preserved on the seafloor. The absence of modern turbidites (≤15 years) in the submarine fan is interpreted to result from bottom current reworking, bioturbation, and the dilution of turbidity currents as they become unconfined on the submarine fan. This study highlights that bottom currents can extensively remobilize turbidites, resulting in a largely incomplete record of turbidity currents on submarine fans. Consequently, caution is needed when reconstructing their recurrence and sediment dynamics using sediment cores, particularly in such dynamic nearshore systems.

1. Introduction

Submarine canyons connect continental shelves and nearshore environments to deeper depositional environments such as submarine fans (e.g., Shepard and Marshall, 1973; Posamentier and Vail, 1988; Gagné et al., 2009; Puig et al., 2013; Normandeau et al., 2014; Hage et al., 2018). Turbidity currents play a key role in their formation and morphology, influencing both their incision into the continental slope and the development of channel features such as meanders and terraces (Shepard and Marshall, 1973; Shepard, 1981). These gravity-driven flows efficiently transport clastic sediments to the deep sea, reshaping the seafloor through erosion and deposition and forming characteristic deposits such as turbidite beds and channel fills (e.g., Meiburg and Kneller, 2010; Piper and Normark, 2009; Talling et al., 2012). Turbidity currents and their deposits have been extensively studied, due to their significance in sediment and carbon transport, hydrocarbon reservoir

* Corresponding authors at: Institut des sciences de la mer (ISMER), Université du Québec à Rimouski (UQAR), Québec-Océan, 310 All. des Ursulines, Rimouski, QC G5L 2Z9, Canada.
E-mail addresses: florian.jacques@uqar.ca, florian.jacques27@gmail.com (F. Jacques), jeancarlos_monteroserrano@uqar.ca (J.-C. Montero-Serrano).

https://doi.org/10.1016/j.margeo.2025.107660
Received 4 May 2025; Received in revised form 19 September 2025; Accepted 25 September 2025
Available online 26 September 2025

formation, impacts on benthic ecosystems, and risks to submarine infrastructure (e.g., Heezen and Ewing, 1952; Meiburg and Kneller, 2010; Talling et al., 2012; Wells and Dorrell, 2021; Bigham et al., 2021). Understanding their triggers, flow dynamics, and factors influencing the completeness of the sedimentary record remains a topic of global scientific interest.

Turbidity currents can be triggered by a variety of mechanisms, including seismic activity, storms, and sediment collapses resulting from geotechnical instabilities (e.g., Piper and Normark, 2009; Puig et al., 2014). Understanding turbidity current dynamics has traditionally relied on sedimentological studies, where flow processes are reconstructed from deposits preserved on the seafloor (Piper and Normark, 2009). This knowledge has been further advanced through physical and numerical modeling, and more recently, through direct observations of turbidity currents (e.g., Hughes Clarke, 2016; Azpiroz-Zabala et al., 2017, Talling et al., 2023). However, direct links between observed turbidity currents and their resulting deposits remain limited (e.g., Stacey et al., 2019). In many cases, the activity of a submarine canyon is assessed by sediment core records from submarine fans, which serve as proxies for depositional processes within the canyon (Amundsen et al., 2015; Fauquembergue et al., 2019). Yet, turbidite recurrence tends to decrease in deeper, more distal settings, and canyon systems may undergo multiple evolutionary phases, including erosion, active deposition, sediment bypass and passive infill (e.g., McHargue et al., 2011; Sumner et al., 2012; Hubbard et al., 2014; Tang and Piper, 2020). In addition, submarine canyons are shaped not only by turbidity currents but also by a range of oceanographic and hydrodynamic processes, such as upwelling, downwelling, tides, internal waves, and other bottom currents. These processes interact with coastal dynamics (including coastal remobilization, storms, and both sudden and continuous sediment supply) and significantly influence sediment redistribution and ecosystem functioning (Puig et al., 2013, 2014; Normandeau et al., 2024; Fernandez-Arcaya et al., 2017). Regional oceanographic conditions, particularly at canyon heads, play a key role in controlling patterns of erosion, deposition, and sediment transport (Li et al., 2019). Despite their importance, many of these processes have seldom been examined in the sedimentary record (Pomar et al., 2012), and the role of bottom currents in canyon systems remains poorly understood, even though they form an important component of sediment dynamics (Li et al., 2019; Miramontes et al., 2020; Normandeau et al., 2024).

In the Lower St. Lawrence Estuary (LSLE; eastern Canada), turbidity currents have been observed in the sediment-starved Pointe-des-Monts (PDM) canyon system (Fig. 1) every few years following sustained storm conditions (Normandeau et al., 2022, 2020). However, the extent to which this activity is preserved in the sediment record is poorly understood.

This study attempts to link deposits preserved in box cores along the main axis of a canyon to processes observed by acoustic moorings and repeat multibeam bathymetry in the canyon. A multiscale dataset from PDM canyons, such as from an acoustic Doppler current profiler (ADCP), multibeam bathymetry from 2007 to 2022, and sediment cores, is used to determine whether turbidity current deposits are preserved in the sediment record and to identify the factors influencing this preservation on the submarine fan. This wide range of multiscale data obtained through different techniques allows us to address the following key questions: 1) Do the various methods used to identify turbidity currents yield consistent interpretations of sediment dynamics? 2) Does the recurrence of turbidites observed on the seafloor accurately reflect turbidity current activity within the PDM submarine canyon? 3) What is the influence of sediment remobilization by bottom currents on the preservation of deposits in submarine fans?

2. Regional setting

The PDM submarine canyons are located at the confluence between the LSLE and the Gulf of St. Lawrence (Fig. 1). The water column of the LSLE (near PDM; Fig. 2) is divided into three water masses during summer: a surface layer until a water depth of 50 m (salinity ≈ 25 ‰; temperature from 2 to 10 °C); a cold intermediate layer from a water depth of 50 to approximately 150 m (salinity ≈ 32 ‰; temperature from −1 to 2 °C); and a bottom layer under a water depth of 150 m (salinity ≈ 33–35 ‰; temperature from 2 to 6 °C; Dickie and Trites, 1983; de Vernal et al., 2011; Galbraith, 2006; Koutitonsky and Bugden, 1991). During winter, the water column is divided into an upper layer with a temperature of approximately 0 °C and a bottom layer with a temperature ranging between 3 and 7 °C (Drinkwater and Gilbert, 2004). Moreover, the LSLE is usually covered by sea ice for 2–3 months during winter. However, the extent and duration of this sea ice cover can vary significantly from year to year. For example, during the winter of 2021, sea ice in the LSLE was nearly absent (Galbraith et al., 2022). The semidiurnal tide has an average tidal range of 3 m in the LSLE and PDM. According to Koutitonsky and Bugden (1991), the wind, tide and runoff of rivers are the main processes impacting the hydrodynamics of the LSLE. Moreover, coastal currents are dominantly oriented west-east (e.g., the Gaspé Current and Anticosti Gyre). The Anticosti Gyre, located east of the PDM, is formed by the convergence of the waters of the LSLE and those from the Gulf of St. Lawrence, which come from Labrador through the Strait of Belle Isle (North-East of the Gulf of St. Lawrence; El-Sabh, 1976). This mixing of less saline estuarine waters with the more saline waters of the Gulf of St. Lawrence causes the formation of a salinity front with a cold front east of the PDM, which expanded from PDM toward the South Shore of the LSLE (Sheng, 2001; Tang, 1980).

Two anticyclonic eddies occur west of PDM, between PDM and Rimouski and between PDM and Baie-Comeau. They are attributed to a bifurcation of the Gaspé Current toward the North Shore and to variable discharges in June and July of the St. Lawrence River, Saguenay Fjord and Manicouagan River. Those eddies can also be affected by storms (Koutitonsky et al., 1990). Additionally, a transverse surface current occurs between PDM and the South Shore of the LSLE, with currents reaching up to 0.35 $m.s^{-1}$ resulting from the North Shore jet (El-Sabh et al., 1982; Farquharson, 1966; Koutitonsky et al., 1990; Tang, 1980). When the Gaspé Current does not bifurcate toward the North Shore, a cyclonic eddy takes place between Rimouski and PDM instead of an anticyclonic eddy (Mertz et al., 1989). Large surface water inflows from the Gulf of St. Lawrence reach the LSLE via the PDM section (Lavoie et al., 2016).

Furthermore, hydrodynamic processes in the LSLE facilitate the occurrence of internal waves (Cyr et al., 2015; Saucier and Chassé, 2000) and upwelling in the PDM area (Forrester, 1974). Internal waves usually propagate along pycnoclines, with amplitudes of a few ten meters in the LSLE (Bourgault et al., 2007; Boegman and Stastna, 2019). Baccara (2023) identified internal waves at PDM at a depth of around 180 m (02M mooring data, location in Fig. 1). These internal waves can occur almost semidiurnally and have the potential to remobilize sediments when they interact with the seafloor (Boegman and Stastna, 2019; Bourgault et al., 2014). For example, internal waves in the PDM canyon axis have a horizontal velocity of 0.15 $m.s^{-1}$ and can remobilize sediments with fine grain sizes, according to Baccara (2023).

The physiography of the LSLE is characterized by a U-shaped valley called the Laurentian Channel at its center (d'Anglejan, 1990), resulting from differential Quaternary glacial erosion (e.g., d'Anglejan and Smith, 1973; St-Onge et al., 2011). Sedimentation rates have been determined along the Laurentian Channel by Smith and Schafer (1999) and estimated at 0.7 $cm.yr^{-1}$ near the head of the Laurentian Channel and 0.042 $cm.yr^{-1}$ in the Gulf of St. Lawrence, with a sedimentation rate of 0.223 $cm.yr^{-1}$ in the Laurentian Channel between the PDM and Saint-Anne-des-Monts. Many submarine canyons and channels incise the LSLE shelves (Gagné et al., 2009; Pinet et al., 2011; Normandeau et al., 2015). A classification of these submarine canyons into four groups was established by Normandeau et al. (2015). In this classification, the PDM submarine canyon system is considered an active sediment-starved system because little sediment is supplied from the coast to the

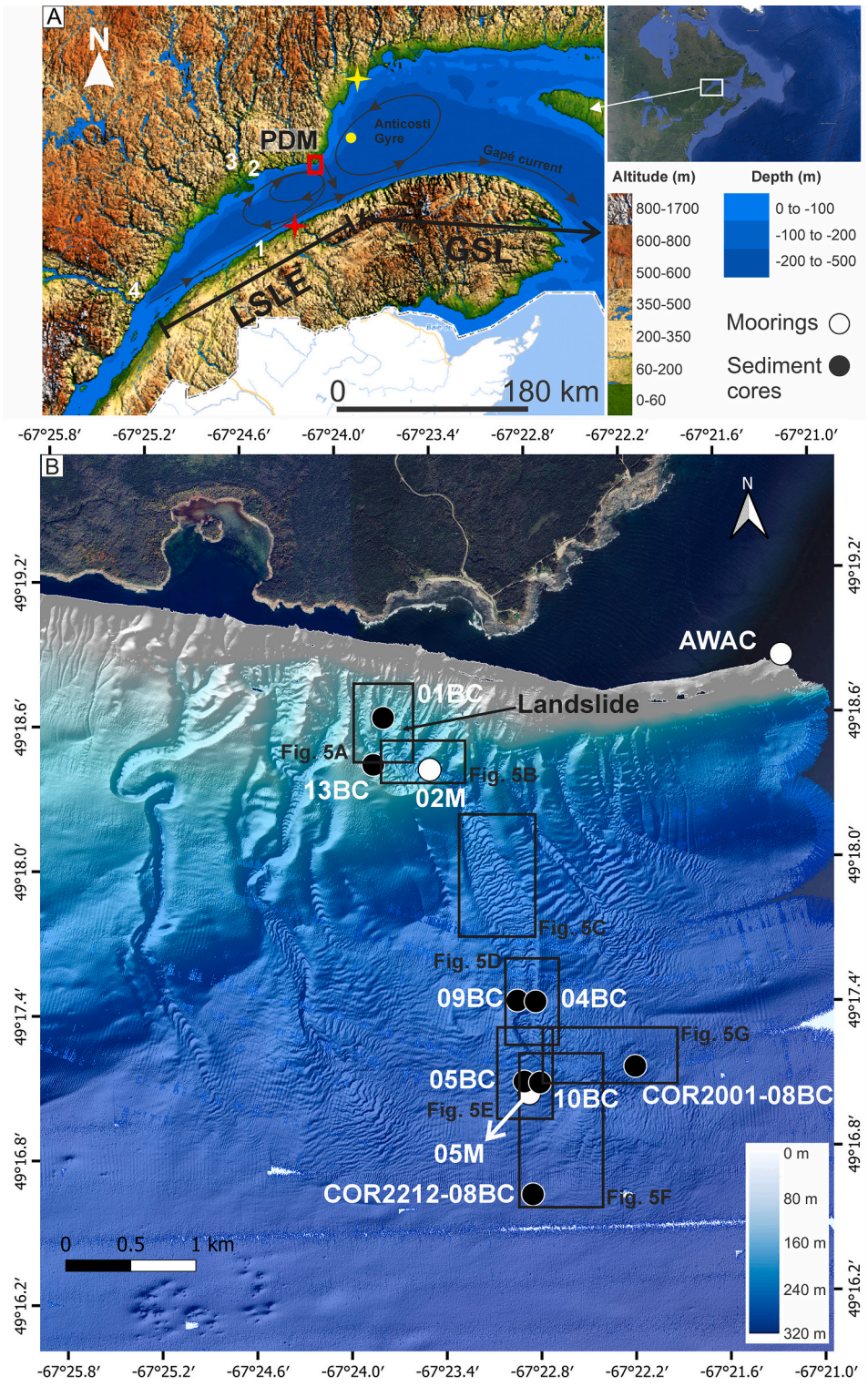

Fig. 1. A) Location of the PDM canyon system in the Lower St. Lawrence Estuary in eastern Canada (red rectangle), location of map A) in North-Western America (white rectangle) and B) multibeam bathymetric map of the PDM canyon system in 2020 with the locations of the sediment cores (black dots) and moorings (white dots). Mooring 05M from Sharpe et al. (2023). The yellow star shows the location of Rivière-Pentecôte (Gulf of St. Lawrence), and the red star indicates the location of Saint-Ulric (Lower St. Lawrence Estuary). The black curves and ellipses represent major regional currents (e.g., El-Sabh, 1976; Faquharson, 1966; El-Sahb et al., 1982; Koutitonsky et al., 1990; Tang, 1980). The yellow dots in Fig. A indicate the epicenter of the magnitude 5.5 earthquake, 35 km northeast from the PDM in 1880 CE (Lamontagne et al., 2018). 1: Rimouski. 2: Baie-Comeau. 3: Manicouagan River. 4: Saguenay Fjord. 5: Sainte-Anne-des-Monts. Base map A, adapted from MINISTÈRE DES RESSOURCES NATURELLES ET DES FORÊTS, 2023 https://www.donneesquebec.ca/recherche/dataset/carte-du-relief-a-l-echelle-de-1-2-000-000 (For interpretation of the references to colour in this figure legend, the reader is referred to the web version of this article.)

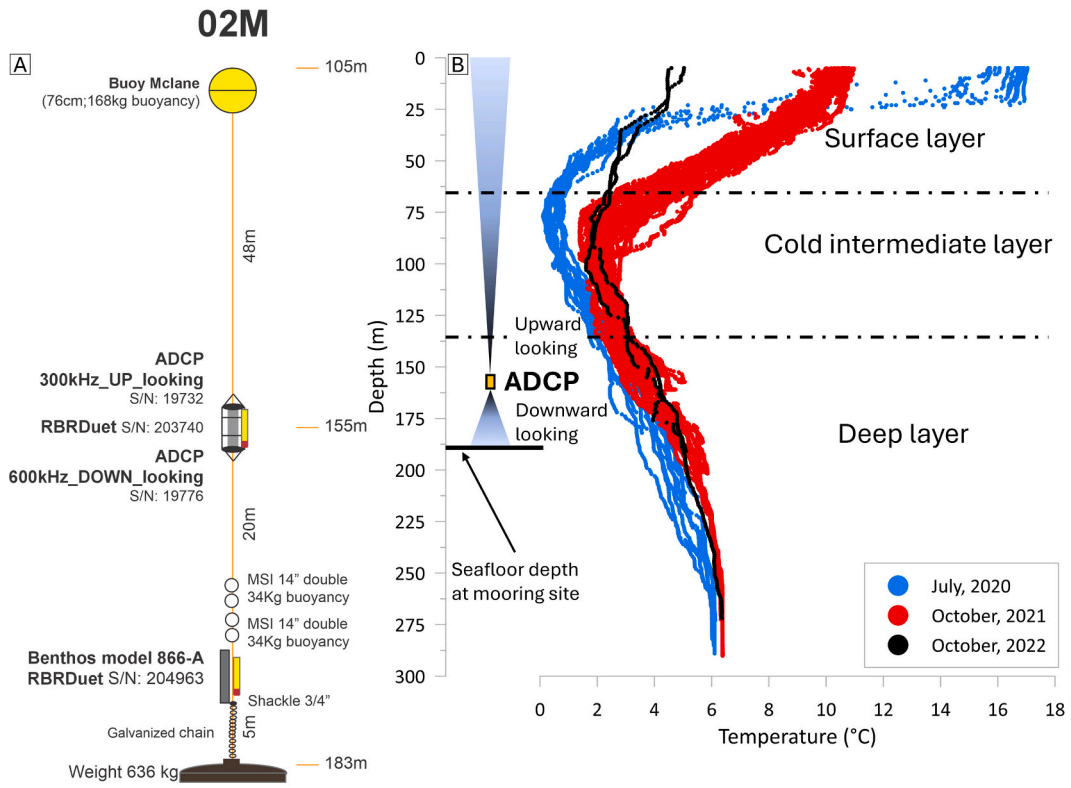

Fig. 2. A) Schematic view of the 02M ADCP-CTD mooring (Limoges et al., 2020), and B) temperature along depth profiles collected around the mooring and in the studied area during July 2020 (COR2001), October 2021 (COR2110), and October 2022 (COR2212).

canyon heads, either by littoral drift or major rivers. Normandeau et al. (2020) reported that the eastern region of PDM is the most active, which is why our data recovery efforts were focused there (Fig. 1).

The PDM submarine canyon system is located less than 300 m from the coastline and consists of mainly rocky shores with only 16 % sandy beaches (Normandeau et al., 2014). The system is approximately 4.5 km long, with canyon widths ranging from 100 to 300 m (Normandeau et al., 2020). As there are no major rivers near PDM, sediment input from the coast is considered low, although sediment can also be transported by nearshore currents and sea ice in the LSLE (Jaegle, 2015).

Crescentic bedforms, interpreted as cyclic steps (Normandeau et al., 2014, 2020, 2022), were observed within the canyons and gullies, along with undulations on the submarine fan. These features suggest the occurrence of recurring turbidity currents within the canyon. Bathymetric surveys conducted in 2007, 2012, and 2015–2019 have previously been used to identify the triggers of turbidity currents (Table 1; Normandeau et al., 2014, 2020, 2022). Turbidity currents have also been directly recorded via acoustic monitoring during major storms (Normandeau et al., 2020). However, storms are not the only mechanism triggering turbidity currents in the LSLE. Merindol et al. (2022) identified turbidity current deposits in sediment cores throughout the LSLE, which were linked to large earthquakes. Moreover, as it is situated in the Lower St. Lawrence seismic zone (Lamontagne et al., 2003; Mazzoti et al., 2005), the PDM region could also be influenced by earthquakes.

In addition to turbidity currents and internal waves, bottom currents can also remobilize a fraction of seafloor sediments. To our knowledge, no direct measurements of bottom-current velocities are available for the PDM region. However, modeled current data for the broader LSLE and Gulf of St. Lawrence, based on the circulation model of Saucier et al. (2003) and applied to data from 1997 to 2018 period (Simon Senneville, personal communication), provide estimates of bottom-current velocities at a horizontal resolution of 5 km. According to this model, maximum bottom-current velocities during that period ranged from 0.26 m.s^{-1} at 300 m depth to 0.6 m.s^{-1} at 150 m depth. Although the model resolution is insufficient to fully resolve the dynamics of the PDM canyon system, it nevertheless indicates that background bottom currents in the region are capable of sporadically remobilizing deposited sediments.

3. Methodology

Most of the data used in this study were collected during the R/V Coriolis II expeditions COR2001 (July 2020, Montero-Serrano et al., 2020), COR2007 (October 2020, Limoges et al., 2020), COR2110 (October 2021), and COR2212 (October 2022). These expeditions allowed the deployment and recovery of ADCP-CTD and sediment trap moorings, the collection of sediment cores and the completion of three bathymetric surveys. Our hydroacoustic and observational results obtained from these expeditions are then compared to previous bathymetric surveys and 02M mooring (ADCP) observations from Normandeau et al. (2020).

3.1. Bathymetric surveys

Repeat bathymetric data were collected in 2012, 2015, 2017, and 2019–2022 onboard the R/V Coriolis II and the R/V Louis-Edmond Hamelin using a Kongsberg EM-2040 multibeam echosounder (MBES; Normandeau et al., 2014, 2020, 2022; Limoges et al., 2020; Montero-Serrano et al., 2020). Here, we focus only on the data from 2015 to 2022 but compare these data with the previous multibeam bathymetric surveys to examine the recurrence of turbidity currents over time (Table 1). The EM-2040 operated at a frequency of 300 kHz. Static and dynamic calibrations (patch tests) were conducted at the beginning of each expedition. Sound velocity profiles (SVPs) were obtained with an AML Minos sensor to calibrate ray tracing of the MBES data. Corrections were applied during data acquisition using SIS and post-processed using the CARIS software, resulting in a horizontal resolution of two meters.

Table 1
Summary of turbidity current observations from 2007 to 2022 in the PDM submarine canyon system. This information was inferred from direct ADCP monitoring and repeated multibeam bathymetric surveys (data from Normandeau et al., 2014, 2020, 2022, and this study). Note that turbidity currents that did not lead to bedform migration could not be identified between bathymetric surveys but likely occurred.

Year	Turbidity currents	Number of turbidity currents	Timing of events	Turbidity current with dense basal layer	Notes
2007–2012	Yes	Unknown	Unknown	Yes	Bedform migration Normandeau et al. (2014)
2012–2015	Yes	Unknown	Unknown	Yes	Bedform migration
2015–2016	No	0	–	–	No bedform migration
2016–2017	Yes	4	12/11/2016 04/01/2017 25/01/2017 15/03/ 2017	'1'	Bedforms migration Mooring displacement Normandeau et al. (2020)
2017–2018	No	0	–	–	No bedform migration
2018–2019	Yes	Unknown	–	Yes	Bedform migration Normandeau et al. (2022)
2019–2020	Yes	Unknown	Unknown	Yes	Bedform migration Normandeau et al. (2022)
2020–2021	Yes	1	03/02/2021	No	No bedform migration Dilute turbidity current
2021–2022	No	0	–	–	No bedform migration

Seafloor movements and differences between the positions of bedform crests were calculated using QGIS.

3.2. Moorings and meteorological data

A mooring (02M) was deployed for two consecutive years, from October 2020 to October 2021 and October 2021 to October 2022, upstream of the main PDM canyon at a water depth of 183 m (Figs. 1 & 2; Table 2). The 02M mooring was equipped with a downward-looking RDI Workshorse Sentinel 600 kHz ADCP, deployed at 30 m above the bottom. This instrument recorded water velocity, acoustic backscatter, and pressure every 20 s for the downward-looking ADCP, with a vertical bin size of 1 m for downward-looking ADCP (Limoges et al., 2020). Each ADCP ping was recorded individually, with the acoustic beams oriented at a 20° angle relative to the vertical angle. The backscatter intensity data were corrected for spherical spreading and water attenuation (Lurton, 2010), then analyzed and visualized in Matlab (version R2012A). We use an arbitrary scale to present backscatter amplitude expressed in dB. Hydrodynamic events, such as turbidity currents, were primarily identified by an increase in backscatter data and associated with an increase in velocity. Only the data of the first ADCP beam is shown. Additionally, RBR CTD sensors were attached to the 02M mooring at depths of 28 m and 6 m above the seafloor, where they recorded water temperature and pressure every 3 s.

Meteorological data from the PDM weather station, such as rainfall, wind velocity and wind direction, were obtained from the Government of Canada website on climatological historical data (Government of Canada, 2024a). The percentage of ice cover off PDM during the years of ADCP monitoring was obtained by compiling each daily ice chart from those years provided by the Ice Service Archive of Environment and Climate Change Canada (Government of Canada, 2024b; https://www.canada.ca/en/environment-climate-change/services/weather-manuals-documentation/manice-manual-of-ice/chapter-3.html). The total concentration of sea ice symbols was transferred out of 100 to translate the code into a sea-ice cover percentage for the PDM area only. The percentage of ice cover off PDM obtained is in accordance with the seasonal maximum ice estimation from Galbraith et al. (2024). Surface waves were measured with a Nortek AWAC-AST 600 kHz ADCP, which was installed upward looking at 2.2 km east of Pointe-des Monts in 40 m water depth (Table 2).

3.3. Sediment sampling

Sediment cores were recovered using a box coring system along the

Table 2
Information about the moorings used or discussed in this study. Locations are illustrated in Fig. 1.

Deployment dates	Name	Deployment depth (m)	Mooring type	Location
Oct 2020 – Oct 2021 Oct 2021 – Oct 2022	02M	Anchoring depth: 183 m ADCP-CTD: 155 m	ADCP-CTD mooring	49°18′23.34″N 67°23′25.98″W
Oct 2020 – Oct 2021 Oct 2021 – Oct 2022	05M	Anchoring depth: 282 m 1st CTD-sediment trap: 155 m 2nd CTD-sediment trap: 225 m	CTDs and Sediments traps mooring	49°17′2.28″N 67°22′50.70″W
Oct 2020 – Oct 2021 Oct 2021 – Oct 2022	AWAC	Anchoring depth: 40 m	ADCP and directional wave gauge mooring	49°18′50.34″N 67°21′11.40″W

Table 3
Information about the cores used in this study. Locations are illustrated in Fig. 1.

Expedition	Name	Water depth (m)	Sediment core length (cm)	Location
COR2212	COR2212-01BC	159 m	8 cm	49°18′36.47″N 67°23′43.30″W
COR2001	COR2001-13BC	152 m	17 cm	49°18′24.84″N 67°23′47.40″W
COR2001	COR2001-09BC	266 m	28 cm	49°17′25.44″N 67°22′54.48″W
COR2212	COR2212-04BC	266 m	27 cm	49°17′25.12″N 67°22′47.56″W
COR2001	COR2001-10BC	277 m	33 cm	49°17′4.92″N 67°22′46.56″W
COR2212	COR2212-05BC	280 m	38 cm	49°17′5.24″N 67°22′52.48″W
COR2001	COR2001-08BC	290 m	45.5 cm	49°17′8.52″N 67°22′10.20″W
COR2212	COR2212-08BC	301 m	47 cm	49°16′37.12″ 67°22′50.13″W

main PDM canyon and its submarine fan during the 2020 and 2022 expeditions onboard the R/V Coriolis II (Fig. 1, Table 3; Montero-Serrano et al., 2020). PVC tubes with a diameter of 10 cm and a length of 60 cm were used to extract a push core sample from each box core using a vacuum pump to minimize compaction. The samples were stored at 4 °C until subsequent physical and sedimentological analyses.

3.4. Physical properties

All cores were scanned using a GEOTEK X-ray computed tomography (X-CT) system at ISMER and the Geological Survey of Canada (Atlantic) to obtain respectively digital X-ray images and laminography slices of the cores, which helped identify sedimentary structures (McDonald et al., 2022). The wet bulk density of whole cores was measured at 0.5 cm intervals using a GEOTEK Multi-Sensor Core Logger (MSCL) at ISMER. The wet bulk density was used as an indicator of lithological changes (e.g. St-Onge et al., 2007), guiding the selection of the best-preserved push cores from each box core. The sediment cores were then split, visually described, and photographed at high resolution. Next, the low-field volumetric magnetic susceptibilities (k_{LF}) were measured at 0.5-cm intervals using a Bartington MS2E, and diffuse spectral reflectance was measured using a Konica Minolta CM2600d.

3.5. Grain size analyses

Grain size analyses of the sediment cores (<2 mm fraction) were conducted at 1 cm intervals using a Malvern-Panalytical Mastersizer 3000 particle size analyzer equipped with a HydroLV module, following the instrumental protocol outlined by Belzile and Montero-Serrano (2022). Prior to analysis, the sediment samples were pretreated with 25 mL of hydrogen peroxide (H_2O_2; 30 %) and 10 mL of hydrochloric acid (HCl; 1 M) to remove organic matter and biogenic carbonates, respectively, and to isolate the detrital fraction of the sediment. The samples were then diluted with approximately 60 mL of Calgon solution (1 % sodium hexametaphosphate), sieved at <2 mm and disaggregated using an in-house rotator for 12 h before grain size analysis. The grain size composition (clay, silt, and sand) and statistical parameters (e.g., sorting, D_{50}) were extracted using GRADISTAT software version 9.1 (Blott and Pye, 2001).

3.6. Lead-210 sediment chronology

The chronology of cores COR2212-05BC and COR2212-08BC were established through ^{210}Pb measurements. Prior to analysis, the sediment samples were sieved through 150-μm Nitex® mesh, dried in an oven at 60 °C, ground and homogenized with an agate mortar to eliminate biases in the ^{210}Pb data associated with variations in the bulk grain size. ^{210}Pb measurements were carried out via alpha spectrometry at the Radiochronology Laboratory of the Geotop Research Center in Montréal, Canada (Ghaleb, 2009). To develop the most accurate age–depth model for the sediment cores, we applied the Constant Flux Constant Sedimentation (CFCS) model (Goldberg, 1963; Krishnaswamy et al., 1971). The sedimentation rates were estimated from the slope of the regression line of excess ^{210}Pb ($^{210}Pb_{ex}$) within the range corresponding to radioactive decay. Data points affected by sediment mixing were excluded from the regression analysis to ensure reliable age–depth estimates.

4. Results and interpretations

4.1. Mooring data (2020−2022)

Turbidity current. – Downward-looking ADCP observations of backscatter (echo intensity) and velocity during the two-year deployment of the mooring 02M (2020–2021 and 2021–2022) revealed only one turbidity current, which occurred on February 3, 2021 (Fig. 3A-C). This event coincided with a storm characterized by sustained winds exceeding 60 km.h^{-1} from north to northeast, along with precipitation and a rise in significant wave height to approximately 6 m (Fig. 4). Two distinct pulses were observed, separated by approximately 40 min (Fig. 3A-C). The nearbed maximum current velocities were 0.6 m.s^{-1} and 0.8 m.s^{-1}, respectively. The first pulse was brief, whereas the second pulse lasted more than 1 h and produced a plume that lofted from the seafloor and reached a height of 25 m above the seafloor. During this turbidity current, the LSLE was ice free in the PDM region.

Sediment resuspension events and other hydrodynamic signals. – In addition to the turbidity currents, two major sediment resuspension events were observed in mooring 02M: one on December 22–23, 2020 (Fig. 3D), which lasted approximately 30 h, and another on March 6, 2021 (Fig. 3E), lasting 7 h. These events were not associated with turbidity currents, as indicated by their internal structure, lower acoustic backscatter, and reduced velocities. However, they resulted in sediment resuspension that was more confined to the bottom of the water column at the mooring site, sometimes following storm activity. Furthermore, three diluted sediment plumes interpreted as potential minor resuspension events were recorded on December 13–14, 2020, January 17, 2021, and March 2–3, 2021 (Fig. S1), with the first two occurring shortly after a storm event, and the three occurring shortly (between less than 4 to 17 days) before the two major resuspension events of December 22–23, 2020 and March 6, 2021 (Fig. S1).

In addition to turbidity currents and resuspension events, the ADCP recorded other sediment transport events whose origin could not be clearly identified. Unlike resuspension events, which are typically confined to the bottom of the water column, these transport events affected broader vertical layers and were not limited to near-bottom dynamics. At mooring 02M, they were characterized by elevated acoustic backscatter, suggesting sediment movement potentially originating from the upper water column. These events influence sediment dynamics by transporting sediment, as evidenced in mooring 02M by elevated acoustic backscatter potentially originating from the upper water column. A notable example occurred on April 17, 2021 (Fig. 3F), lasting approximately 45 min and primarily impacting the upper part of the water column at the 02M mooring site. Due to its structure, the nature of this event remains uncertain. No turbidity currents were recorded during the second year of deployment of mooring 02M.

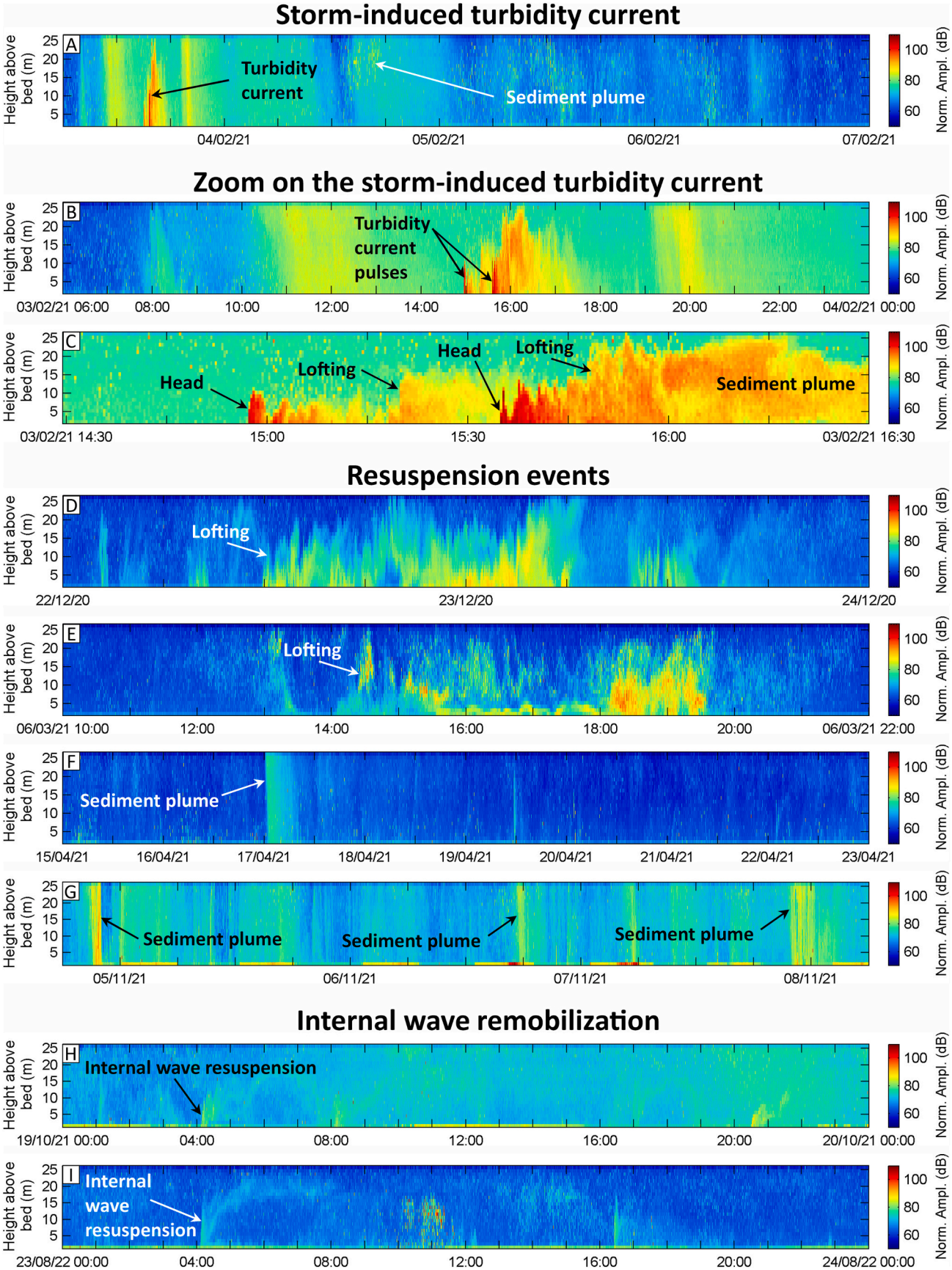

Fig. 3. Backscatter data of a storm-induced turbidity current (A), zoomed-in view of the 03/02/2021 turbidity currents (B), (C), remobilization events (D), (E), (F), (G) and examples of internal waves (H), (I), recorded during the two years by the downward-looking ADCP at mooring 02M. (A): 03/02/2021. (B): 03/02/2021. (C): 03/02/2021. (D): 22/12/2020. (E): 06/03/2021. (F): 17/04/2021. (G): 04–08/11/2021. (H): 19/10/2021. (I): 23/08/2022.

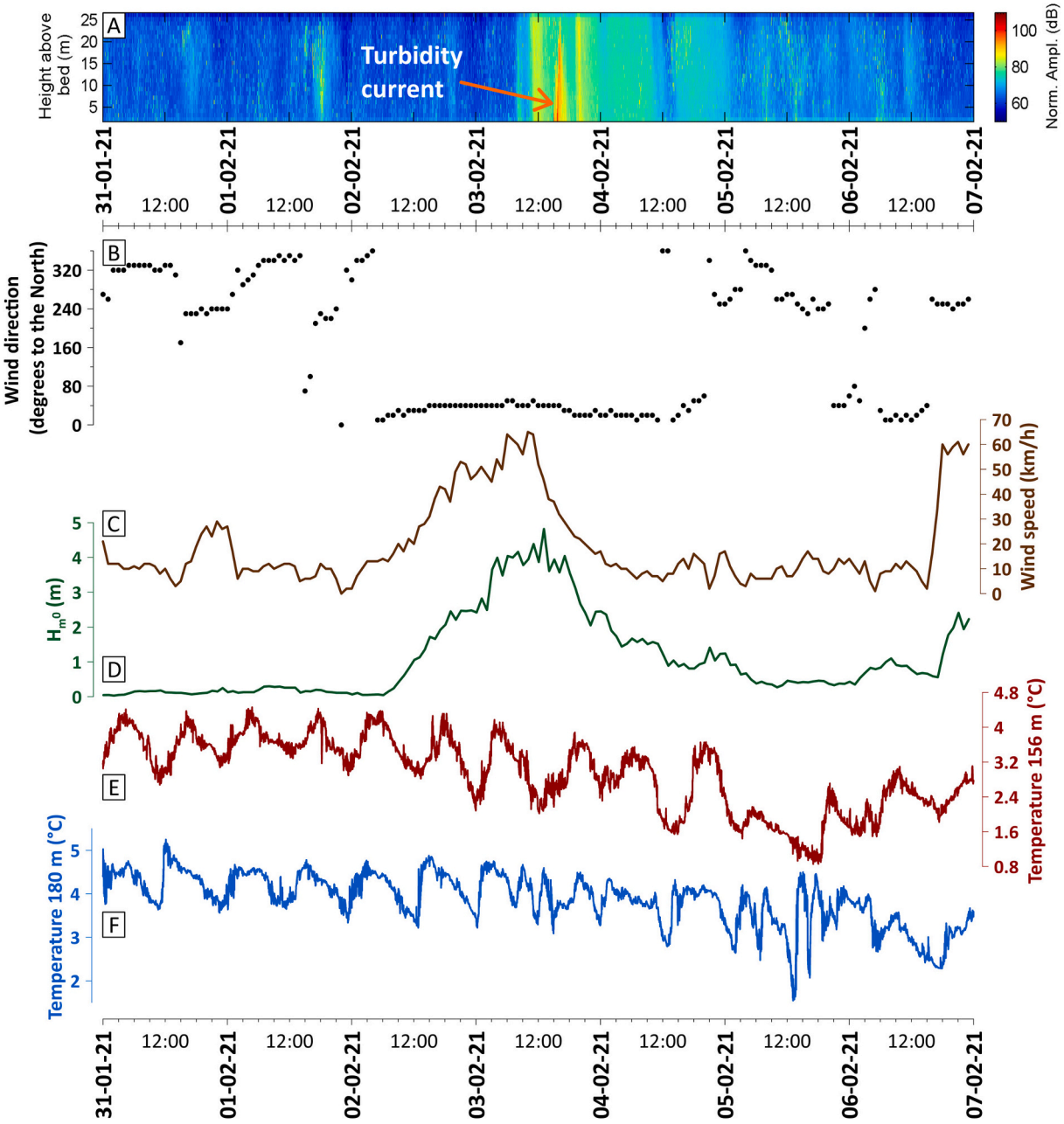

Fig. 4. Time series from January 31 to February 7, 2021, illustrating changes in key parameters associated with and potentially triggering the turbidity current event on February 3: A) backscatter intensity, B) wind direction, C) wind speed, D) significant wave height H_m^0 (calculated via the spectral method) measured at Pointe-des-Monts, E) temperature at 156 m, and F) temperature at 180 m. The orange arrow indicates the turbidity current event as detected by backscatter intensity.

However, several sediment transport or small resuspension events were detected (see Fig. S2 for the full year-long backscatter intensity record). The most significant sediment transport event occurred between November 04 and 07, 2021 (Fig. 3G). In addition, substantial sediment transport was observed in April 2022, following spring ice melt in the LSLE and the associated increase in river discharge (Galbraith et al., 2023).

Moreover, in the LSLE and particularly at the PDM region, internal waves are associated with most tidal cycles and lead to sediment resuspension when they interact with the seafloor (Baccara, 2023; Bourgault et al., 2014). These resuspension events are characterized by small to moderate increase in backscatter intensity near the seafloor. According to Baccara (2023), tidal currents in the PDM area are also evident through increased backscatter during periods of strong currents (Fig. 3H, I). Increased backscatter is often linked to sediment suspension and plankton migration in the water column and can be measured at depths of down to 180 m at this ADCP mooring.

4.2. *Repeated bathymetric surveys*

Repeat seafloor mapping conducted in PDM canyon systems between 2015 and 2022 were used to analyze morphological features and their evolution over time (Fig. 5). Data from 2021 are not presented, as differences between 2020, 2021, and 2022 were negligible in the main canyon axis. Since the horizontal resolution of the datasets is 2 m, only changes exceeding this threshold are detectable. Moreover, due to significant vertical errors resulting from challenges in calibrating velocity profiles, steep slopes, and water density variations (Normandeau et al., 2014), our analysis focuses on horizontal changes.

Overall, the eastern part of the system (including the eastern gullies

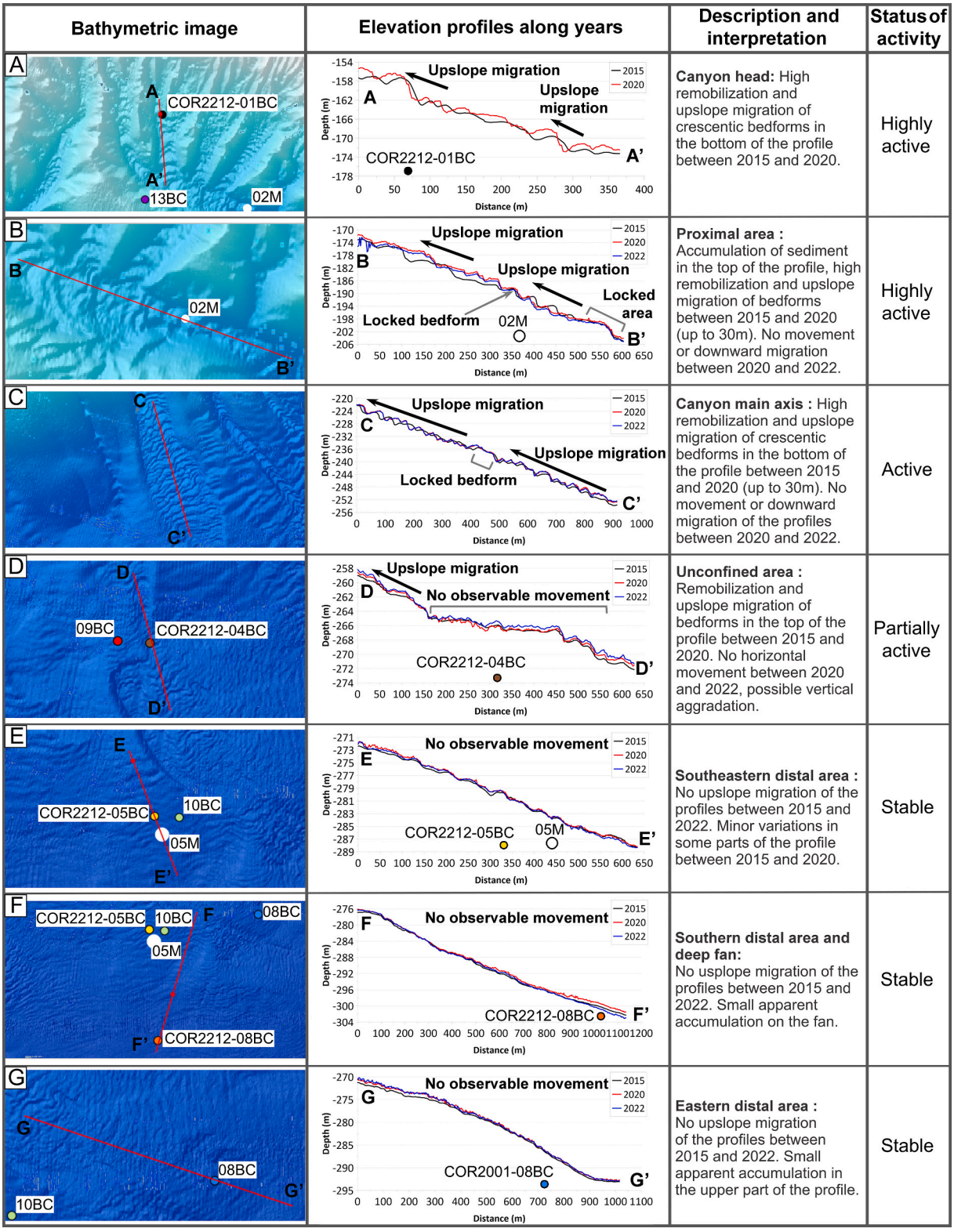

Fig. 5. Elevation profiles along the eastern canyon for 2015, 2020, and 2022, highlighting key areas for studying sediment dynamics. The profiles were taken at strategically selected locations, focusing exclusively on horizontal displacement with a resolution of 2 m. Sediment core locations are shown in the first two columns. The positions of maps A to G are shown in Fig. 1. Apparent accumulations in profile D-G could be artifacts related to improper correction of the multibeam data due to strong variations in sound speed.

and the main canyon axis) was the most active during the monitoring period. Between 2015 and 2020, upward migration of crescentic bedforms was observed at all these locations (location Fig. 1, not shown here). Elevation profiles from 2015 to 2020 along the largest canyon axis and its associated lobe are shown in Fig. 5 and are described below for both the proximal and distal areas:

Proximal area. - Profile A (Fig. 5), located at the head of the canyon, shows upslope migration of crescentic bedforms between 2015 and

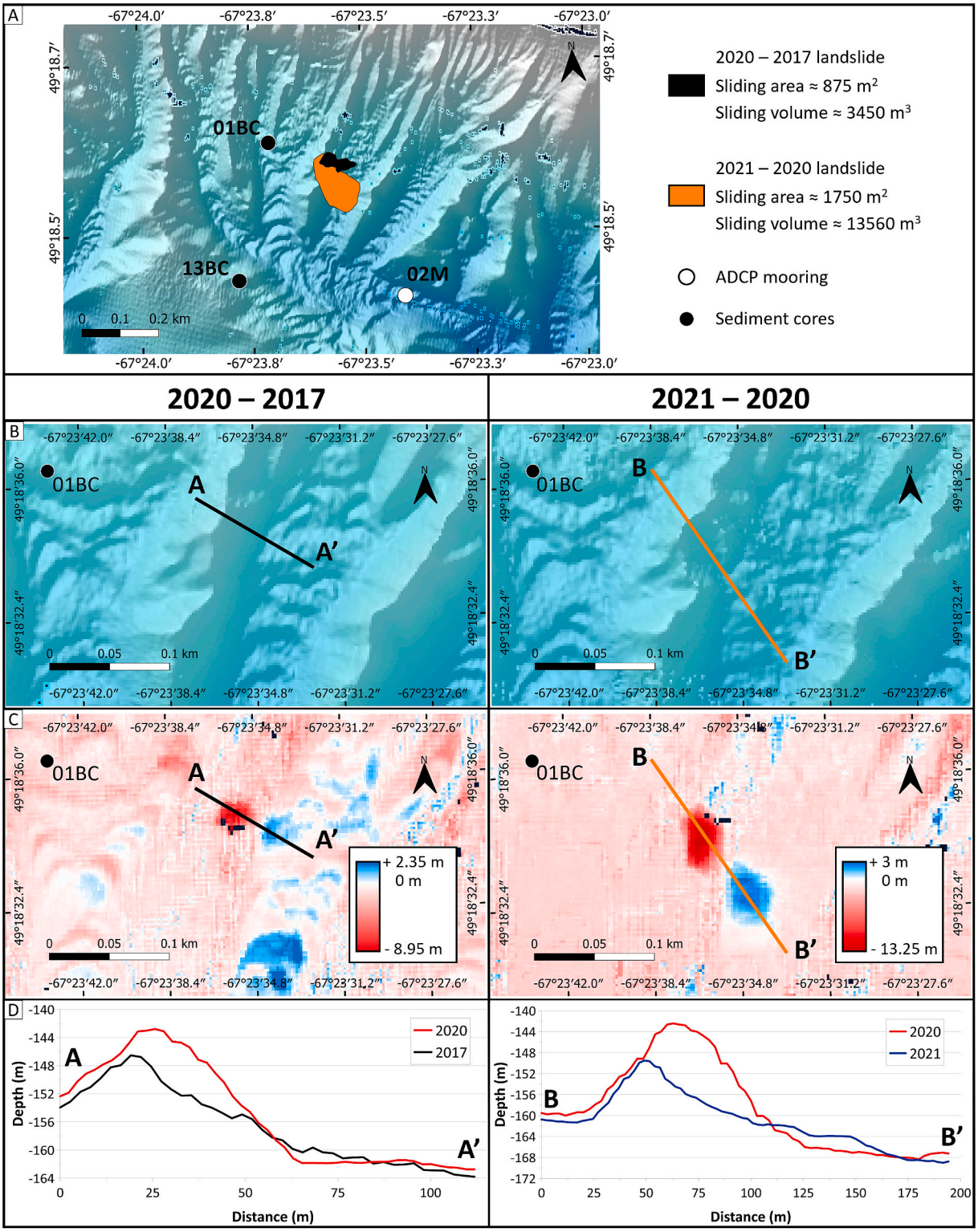

Fig. 6. (A) Locations of landslides within the PDM canyon system. (B) Multibeam bathymetric maps of 2017 (left) and 2021 (right). (C) Depth difference maps illustrating sediment accumulation (blue) and erosion (red) associated with landslides that occurred within a canyon of the PDM submarine canyon system between 2017 and 2020 (left) and between 2020 and 2021 (right). (D) Cross-sectional profiles along the main PDM canyon, highlighting sediment remobilization/erosion on the seafloor. (For interpretation of the references to colour in this figure legend, the reader is referred to the web version of this article.)

2020. Due to the poor quality of the 2022 data in this proximal area, those results are not presented here, although data from 2022 are included for the other distal profiles. A small landslide occurred at the head of the major canyon between 2020 and 2021 at depths of approximately 143 to 161 m, affecting an area of approximately 1750 m^3 with a volume of around 13,500 m^3 and a maximum erosion thickness of up to 15 m (Fig. 6). This channel wall landslide may have been responsible for the small turbidity current event recorded by the ADCP on February 3, 2021 (Fig. 6). Notably, another smaller landslide occurred slightly above this area between 2017 and 2020 (Fig. 6).

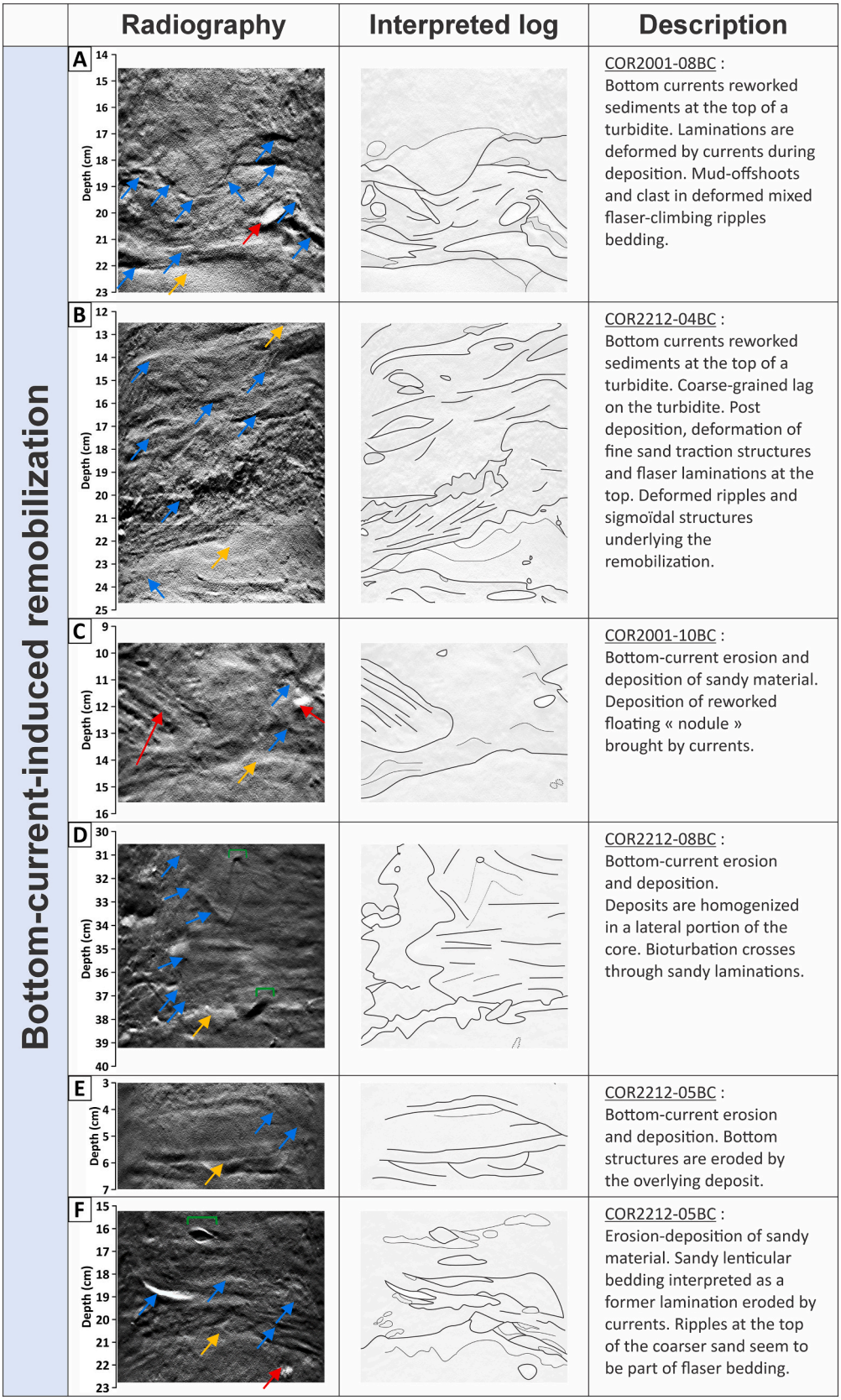

Fig. 7. Close-up of X-ray structures, their line drawings and interpretation. The table uses the same colors as those in the facies log in Fig. 8: blue indicates remobilized sediments (A-F), light brown indicates turbidity current deposits (G-I), and green represents background sedimentation (J-L). The blue arrows underline bottom current remobilization structures or remnants of turbidity current structures. The yellow arrows underline structures associated with turbidity currents. The red arrows indicate clasts and nodules transported by either turbidity currents or bottom currents. The green arrows and brackets represent bioturbation structures and shells. (For interpretation of the references to colour in this figure legend, the reader is referred to the web version of this article.)

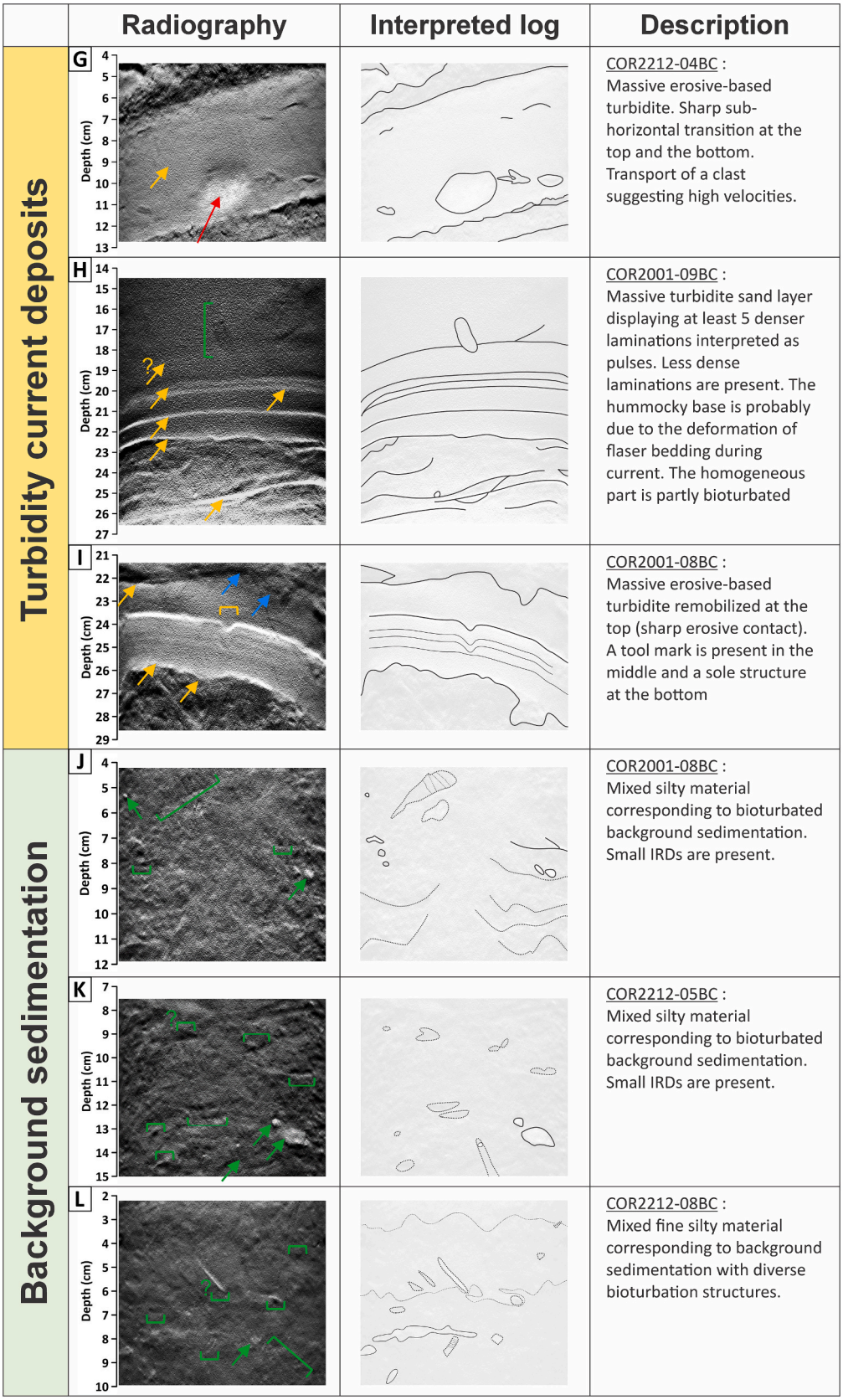

Fig. 7. (*continued*).

Profile B was plotted at the 02M mooring site and indicates a mean upslope migration of bedforms of up to 25 m between 2015 and 2020. Profile C, located in the larger downstream channel, records similar bedform movements. Profile D, situated in the downstream area of the main canyon where sediments become unconfined. In the upstream part of this profile, a mean bedform migration of 10 m was observed between 2015 and 2020. Downstream, no morphological changes are evident from 2015 to 2022.

Distal area. - Profiles E, F and G were strategically positioned on the submarine fan to intersect with coring sites presented in later sections. Considering the 2 m horizontal resolution of the bathymetric datasets, no migration of sediment waves was observed between 2015 and 2022 (Profiles E, F, and G; Fig. 5). Minor morphological changes appear to have occurred between 2015 and 2020, but these remain within the range of instrumental uncertainty. No visible changes were observed between 2020 and 2022, which is consistent with data acquired from the 02M moorings during the same period.

4.3. Sedimentary facies of recent deposits

4.3.1. Sedimentary facies description

Sedimentary deposits in the box cores reveal episodic events of varying magnitudes, often involving post-depositional remobilization. These deposits can be categorized into three main facies: 1) bottom-current-induced remobilization (blue in Fig. 7A-F), 2) turbidity current deposits (yellow in Fig. 7G-I), and 3) background sedimentation (green in Fig. 7J-L).

Sediment remobilization by bottom current is characterized by a median grain size (D_{50}) ranging from approximately 30 to 175 μm. Sorting varies along the deposits depending on the degree of remobilization, with values ranging from ≈ 1.7 to 3.7 μm. The deposits mainly consist of deformed and eroded sedimentary structures and sometimes incorporate allochthonous material. For example, some coarser lenticular layers were interpreted as former laminations that were remobilized by bottom currents during or after deposition. In some cases, deposits appear homogenized in lateral sections of the sediment cores, reflecting post-depositional reworking. A common sedimentary structure observed in our cores is flaser bedding (Fig. 7A,B). However, a variety of other structures are present in several cores, including parallel laminations, climbing ripples, lenticular bedding, sigmoidal structures, mud-offshoots, truncated layers, floating clasts or lenses, and sand lags (Fig. 7A-F). These features are indicative of strong bottom-current reworking (e.g., Rebesco et al., 2014; Shanmugam et al., 1993; Shanmugam, 2003, 2008; Stow and Faugères, 2008; Viana et al., 1998). In addition, the presence of inverse-to-normal grading in many sequences can be attributed to bottom-current-induced remobilization (e.g., Shanmugam et al., 1993; Martín-Chivelet et al., 2008). We also interpret thin coarse-grained laminae with irregular or non-uniform structures, such as those observed at 37–39 cm in COR2212-08BC (Fig. 8), as evidence of reworking by bottom currents.

Turbidity current deposit facies fall into the range of moderately well sorted to poorly sorted sands (≈ 1.5 to 3.4 μm). Poor sorting is typically associated with either the erosive base of the turbidite or with upper layers that have been remobilized or mixed with finer sediments. The median grain size (D_{50}) varies from approximately 105 to 205 μm. These facies are characterized by inverse-to-normal grading in deposits located closer to the coast, and by simple normal grading in those farther offshore. Along the canyon axis, deposits often consist of massive sand with an erosive base, grading into hummocky structures (Figs. 7G-I & 8). On the levee, they display thinly spaced millimetric laminae followed by homogeneous sand. In the submarine fan, turbidity current deposits are composed of erosive-based massive sand, some of which contain climbing ripples, tool marks, or sole structures.

The background sedimentation facies is characterized by relatively homogenous, poorly sorted silt to very fine sand, with a D_{50} ranging from approximately 19 to 90 μm. Occasionally, coarser grains (>500

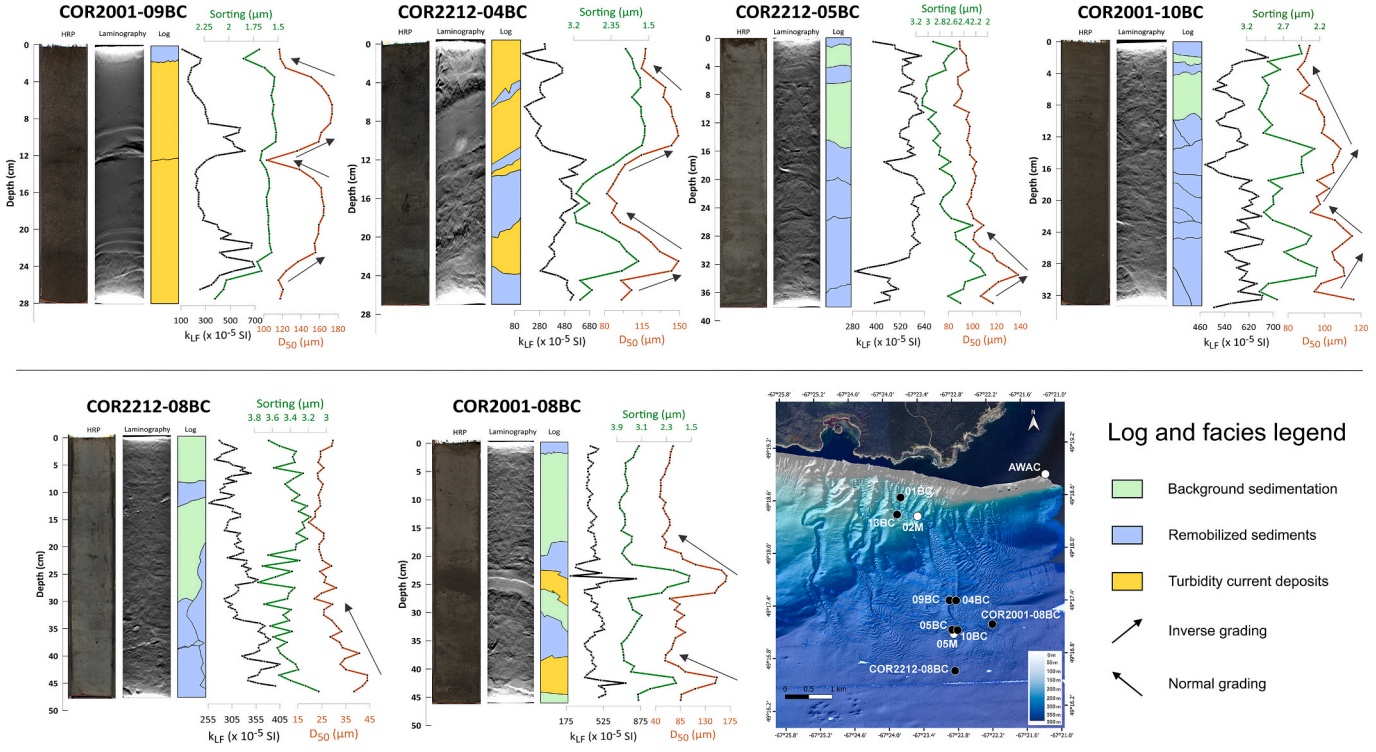

Fig. 8. High-resolution photographs (HRP), X-ray images (laminography), core facies log, magnetic susceptibility (k_{LF} x 10^{-5} SI), sorting (inverted axis) and D_{50} for the six major cores studied here. Each core can be found individually in the supplementary material (Fig. S3 to S10). The profiles for cores COR2212-01BC and COR2001-13BC can be found in the supplementary material (Fig. S11).

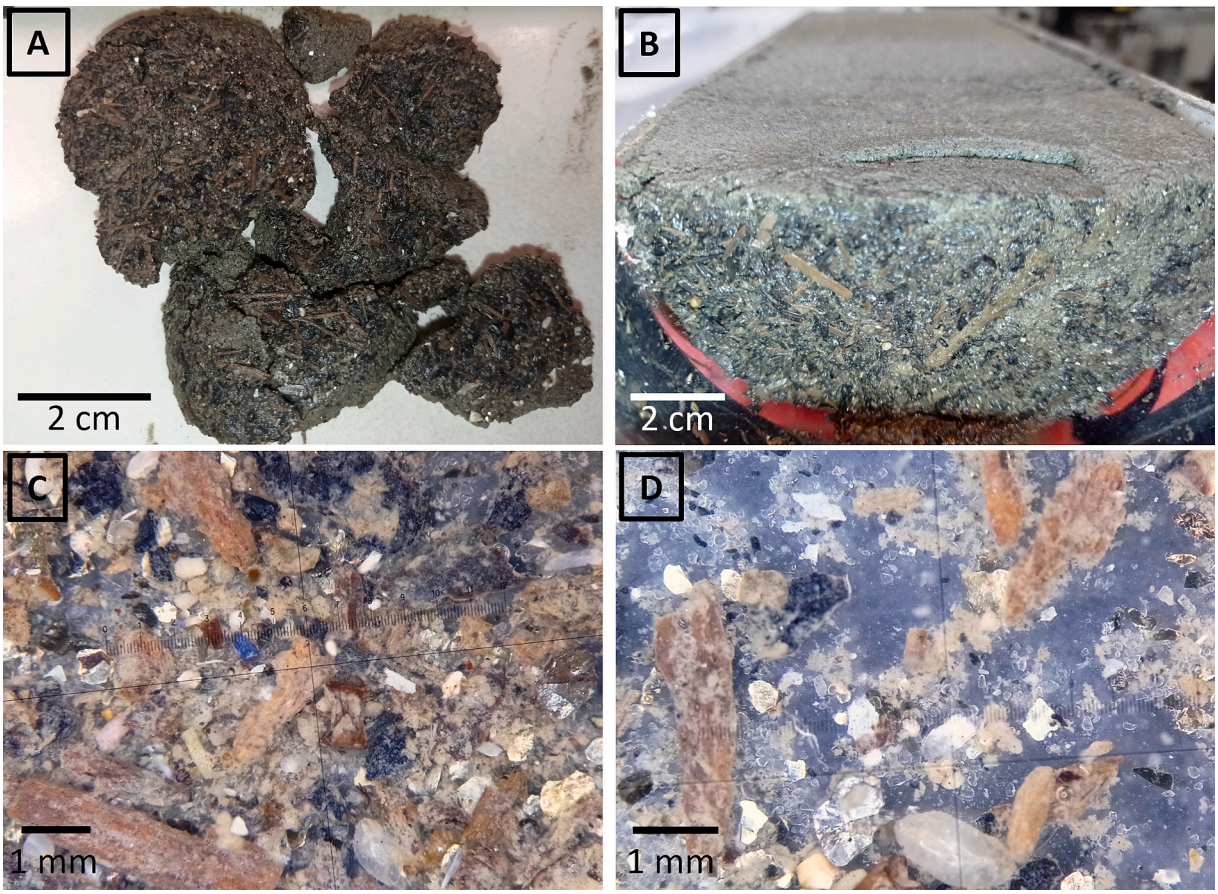

Fig. 9. Organic debris, microfossils, mica minerals, and small rock fragments found at the tops of cores COR2001-09BC and COR2212-04BC. A) View of the top of core COR2001-09BC. B) Half-sectional view of the top of core COR2212-04BC. C) and D) Close-up views of the top of core COR2001-09BC under a binocular microscope.

μm) are present, which may be interpreted as ice-rafted debris (IRD) resulting from annual winter ice. Bioturbation structures are commonly observed in this facies.

4.3.2. *Cores description*

The grain size of sediments within the PDM canyon system generally ranges from coarse silt to fine sand (Fig. 8). Grain size data from sediment cores reveal a classic fining trend with increasing distance from the coast, reflecting reduced hydrodynamic conditions offshore. An exception to this trend is observed in turbidite deposits, which are notably coarser and better sorted (Fig. 8).

Facies distribution in proximal cores. - The two cores collected from the canyon head contain the coarsest sediments. Core COR2212-01BC consists of massive sand and contains fine sand (D_{50} between 184 and 203 μm), fining upward in the top two centimeters. In contrast, core COR2001-13BC shows inverse grading followed by normal grading from depths of 16 to 3 cm, with fine normal grading extending to the top (Figs. S3, S4 & S11). In the main canyon axis, core COR2212-04BC comprises four turbidites (Fig. 8), most of which are characterized by lower massive facies grading into hummocky structures (Figs. 7B,G & 9). On the adjacent levee, core COR2001-09BC contains two turbidites exhibiting inverse grading followed by normal grading (Fig. 8). X-CT images of these turbidites reveal multiple depositional pulses, overlain by homogeneous sand layers (Figs. 7H & 8). Although cores COR2212-04BC and COR2001-09BC were recovered two years apart (October 2022 and October 2020, respectively), both are capped by organic/plant debris (Fig. 9), suggesting little to no sediment deposition during that interval. In addition, grain size data from the core COR2001-09BC are generally coarser than those from COR2212-04BC.

Facies distribution in distal cores. - Core COR2212-05BC contains diverse sedimentary structures with fine sand (D_{50} between 80 and 140 μm), influenced by traction currents in a distal environment, as well as sediment remobilization by bottom currents and bioturbation. The interval from 18 to 38 cm displays inverse followed by normal grading and includes a variety of structures. A sandy lenticule at 18 cm suggests a former lamination or bedding eroded by currents. Ripples at 20 cm seem to be remnants of flaser bedding. These features suggest that a turbidite remnant was remobilized by bottom currents (Figs. 8E-F & 9). Additionally, climbing ripples are observed between 24 and 26 cm, and a small mud-offshoot surrounded by deformed laminations is present between 30 and 32 cm. Between 28 and 38 cm, lightly hummocky structures suggest resuspension during deposition. The nearby core COR2001-10BC shares similar deformed sedimentary structures (Fig. 8). It contains two small deposits with slight inverse grading followed by normal grading, affected by deformation, nodules, and lenticules, which are features indicative of bottom-current remobilization (Figs. 7C & 9). The upper 12 cm of core COR2001-10BC also shows evidence of bioturbation and bottom current influence. In the distal eastern area, core COR2001-08BC is composed of two turbidity current deposits that are remobilized at the top (Figs. 8I & 9). Several sedimentary structures, including laminations, are associated with these turbidity currents. In addition, isolated disturbed sediment deposits are observed between the turbidites. The upper portion of the core is dominated by background sedimentation facies (Figs. 8J & 9). The more distal core, COR2212-08BC (Figs. 8D, L & 9), generally contains the finest grain size among the PDM canyon system cores (D_{50} between 19 and 44 μm). Bioturbation is common throughout most of this core (Figs. 7L & 9). Between 30 and 40 cm, the presence of laminations,

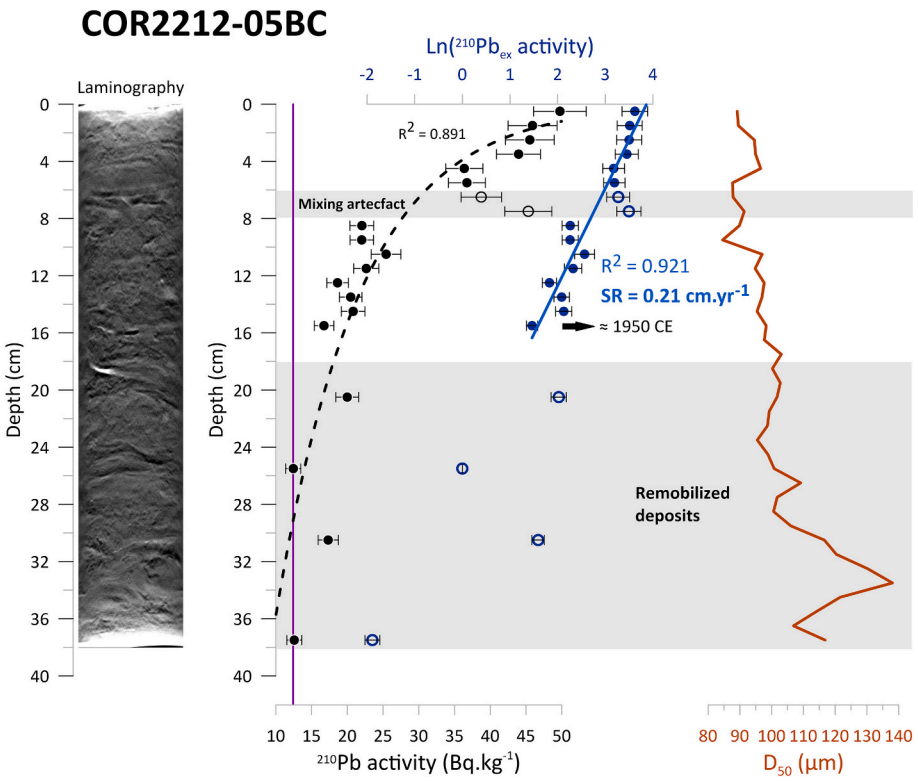

Fig. 10. COR2212-05BC. X-CT laminography, ^{210}Pb activity, Ln($^{210}Pb_{ex}$), and D_{50}. The sedimentation rates (SRs) calculated with the ^{210}Pb activity in the core allow estimation of deposit ages. SRs are calculated from the slope of Ln ($^{210}Pb_{ex}$) by excluding biological mixing and remobilized intervals. The violet vertical bar indicates the $^{210}Pb_{unsupported}$ level. (For interpretation of the references to colour in this figure legend, the reader is referred to the web version of this article.)

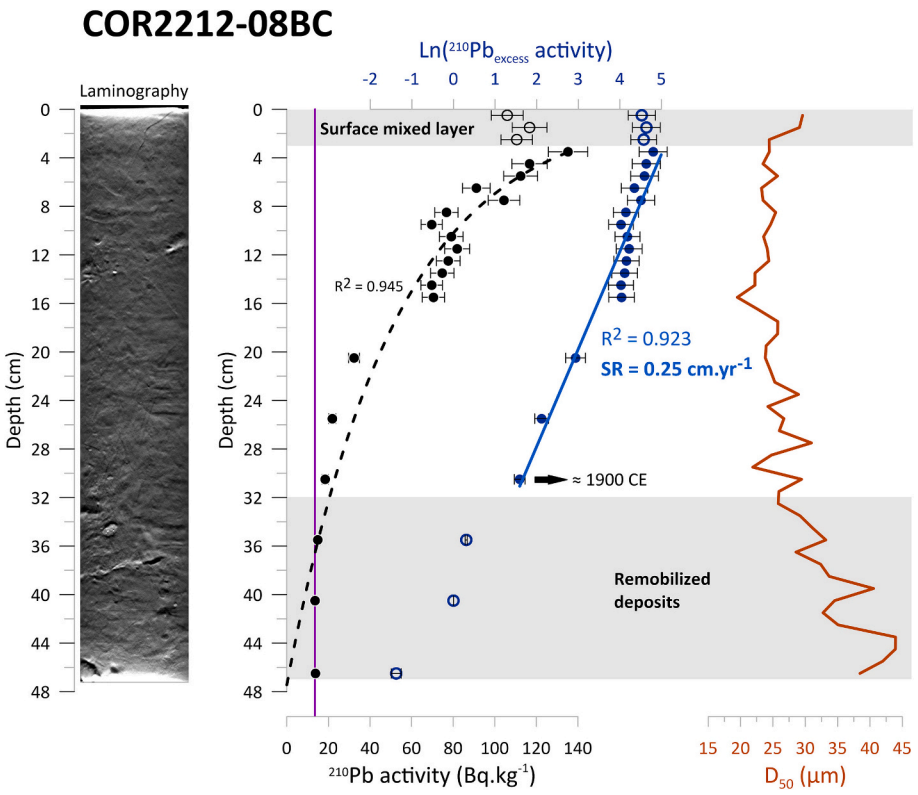

Fig. 11. COR2212-08BC. X-CT laminography, ^{210}Pb activity, Ln($^{210}Pb_{ex}$), and D_{50}. The sedimentation rates (SRs) calculated with the ^{210}Pb activity in the core allow estimation of deposit ages. SRs are calculated from the slope of Ln ($^{210}Pb_{ex}$) by excluding biological mixing and intensely remobilized zones. The violet vertical bar indicates the $^{210}Pb_{unsupported}$ level. (For interpretation of the references to colour in this figure legend, the reader is referred to the web version of this article.)

gravels, and sandy nodules overlying coarser sediments with thin laminae (notably at 37–39 cm) within a normally graded deposit suggests a depositional environment influenced by bottom currents, where potential turbidites were remobilized (Fig. 8).

4.4. Chronology of cores COR2212-05BC and COR2212-08BC

Cores COR2212-05BC and COR2212-08BC exhibit remobilized intervals (COR2212-05BC: 18–38 cm, Fig. 10A; COR2212-08BC: 32–47 cm, Fig. 11A), as well as layers affected by bioturbation (COR2212-05BC: 6–8 cm, Fig. 10A,C; COR2212-08BC: 7–8 cm, Fig. 11A,C). The profiles of $^{210}Pb_{ex}$ activity in both cores display disturbances due to these remobilized layers, with less pronounced disruptions in core COR2212-08BC. To establish an event-free chronology based on ^{210}Pb measurements, turbidites and bioturbated layers were excluded from the age-depth model.

The ^{210}Pb data for COR2212-05BC suggest that the sediment overlying the remobilized deposit highlighted in grey in Fig. 10 spans several decades (Fig. 10). While uncertainties make it challenging to determine the exact age of these sedimentary events using ^{210}Pb data alone, the data indicate that the coarser-grained deposit at 18–37 cm was deposited before 1950 CE (Fig. 10). The mean sedimentation rate of this core is approximately 0.21 cm.yr^{-1}.

The ^{210}Pb profile of COR2212-08BC is less disturbed than that of COR2212-05BC (Fig. 11), probably because of its more distal position in the PDM canyon system and less remobilization. Most of the deviation from the exponential trend in the top 3 cm of the core is attributable to biological mixing (Fig. 11). This intensity of mixing is low enough to provide reliable sedimentation rate data for the top 30 cm of COR2212-08BC (Fig. 11). Deposits between 29 and 32 cm appear slightly remobilized; however, this does not seem to have affected ^{210}Pb behavior to any great extent. Although the exact age of the oldest deposit at 32–47 cm cannot be determined, the model suggests that it could have formed before 1900 CE (Fig. 11). The mean sedimentation rate of this core is approximately 0.25 cm.yr^{-1}. The sedimentation rates for both cores are in accordance with cores from the Laurentian Channel (Smith and Schafer, 1999) and in the range of data from Mérindol et al. (2022) with cores from the slopes of the LSLE.

5. Discussion

5.1. Sediment dynamics inferred from repeated multibeam bathymetric surveys and direct observations

Over the two years of ADCP monitoring presented in this study (2020–2021 and 2021–2022), one turbidity current was detected on February 3, 2021 (Fig. 3A-C). This event was brief, with the plume lasting less than two hours from the initial pulse to dissipation. Based on the absence of upslope migration of cyclic steps between 2020 and 2021, we infer that the turbidity current lacked a dense basal layer (Paull et al., 2018). In previous years, the upward migration of crescentic bedforms, evident from bathymetric surveys, suggests the presence of supercritical turbidity flows with dense basal layer and flows instabilities such as cyclic steps (e.g., Kostic and Parker, 2006; Postma and Cartigny, 2014; Hage et al., 2018; Talling et al., 2023). These conditions promote erosion, sediment redeposition, and seafloor reshaping. In contrast, the absence of bedform migration implies that recent flows were either minor or too diluted to significantly modify the seafloor. These observations highlight the variability of turbidity current activity within the PDM canyon system, which is neither uniform nor constant on an annual basis. This event was therefore minor compared to those previously documented in the same canyon by Normandeau et al. (2020) and in other canyon-channel systems (e.g., Hughes Clarke, 2016).

The turbidity current coincided with a winter storm under ice-free conditions in the LSLE, which generated large wave heights, particularly at the PDM site (Figs. 3D & 12; Galbraith et al., 2024). This observation supports earlier findings that turbidity currents in the PDM area are often storm-triggered (Normandeau et al., 2020).

In addition to this turbidity current, several sediment resuspension events were observed that did not evolve into turbidity currents. Such events also occurred during the nearly ice-free winter of 2020–2021 and under ice-free conditions in 2021–2022, sometimes following storms.

When combined with previously published ADCP and repeated multibeam bathymetric data (Normandeau et al., 2020), our findings indicate that at least nine turbidity currents have occurred in the past 15 years (Table 1), along with several smaller remobilization events occurring on an annual basis (Fig. 3D-G). As shown in Fig. 12, most turbidity currents occurred during winter months under ice-free conditions since 2015 and were storm-induced. In contrast, years with high sea ice concentrations and prolonged winters often lacked recorded turbidity currents (Fig. 12). This pattern suggests that ice-free conditions are more favorable for turbidity current and sediment remobilization events. Surface waves are strongly reduced in presence of sea ice (Squire, 2020), and currents induced by strong winds are also prevented by sea ice. In the future, if the LSLE experiences more frequent ice-free conditions, turbidity currents may become increasingly common as reduced ice cover offers less protection from storm activity.

While some of these smaller events were clearly storm-related, others had no identifiable trigger. It is possible that small slopes instabilities, potentially enhanced by oceanographic processes such as internal waves and tides, contributed to their occurrences. For example, a small channel wall failure was detected in 2021 (Fig. 6), which, although not precisely dated, may have contributed to the turbidity current triggered by February 3, 2021. Alternatively, it could be associated with other minor sedimentary events from that year, such as the one recorded on April 19, 2021 (Fig. 3F). This event dispersed throughout the water column before reaching mooring 02M, with most of the landslide-derived sediments deposited at the base of the canyon wall, directly below the failure area. As demonstrated by Xu et al. (2013), small-scale slope failures can produce small and dilute turbidity currents that spread into the water column. Such processes may have occurred regularly at PDM in the past.

In the more proximal area of the submarine fan, Profile D in Fig. 5 exhibits lower amplitudes of upstream crescentic bedform migration, indicating a decrease in the turbidity current's transport energy. In the more distal part of the profile (Fig. 5D), sediment become unconfined, and no bedform migration is observed. This transition as the canyon loses confinement suggests a hydrodynamic threshold beyond which most turbidity currents slow down, dissipate into the water column, or follow alternative paths across the fan, with velocities too low to mobilize bedforms. A similar interpretation was proposed by Stacey et al. (2019) for the fjord delta system of the Squamish River (British Columbia, Canada). A noticeable decrease in slope at this location further supports a shift in canyon dynamics. This change renders the distal region of the PDM canyon less dynamic, requiring more powerful turbidity currents to reach and reshape the seafloor.

In summary, repeated multibeam bathymetric surveys and 02M mooring data indicate that at least nine turbidity currents affected the PDM canyon system between 2007 and 2022. Additional dilute turbidity currents likely occurred but did not produce measurable seafloor changes or bedform migration, underscoring the variability in flow energy and sediment transport across the canyon system.

5.2. How effectively do sediment cores capture the spatial and temporal variability of modern sediment dynamics

5.2.1. Modern sediment activity inadequately captured by sediment cores

To address the limited temporal coverage of the bathymetric data, sediment cores were collected to extend the record of turbidity current activity within the PDM canyon system. Most core samples exhibit fine sand median grain sizes (D_{50}) consistent with a high-energy near-coastal environment, whereas the distal cores (COR2001-08BC and COR2212-08BC) contain a higher proportion of fine silt (Fig. 8), possibly due to

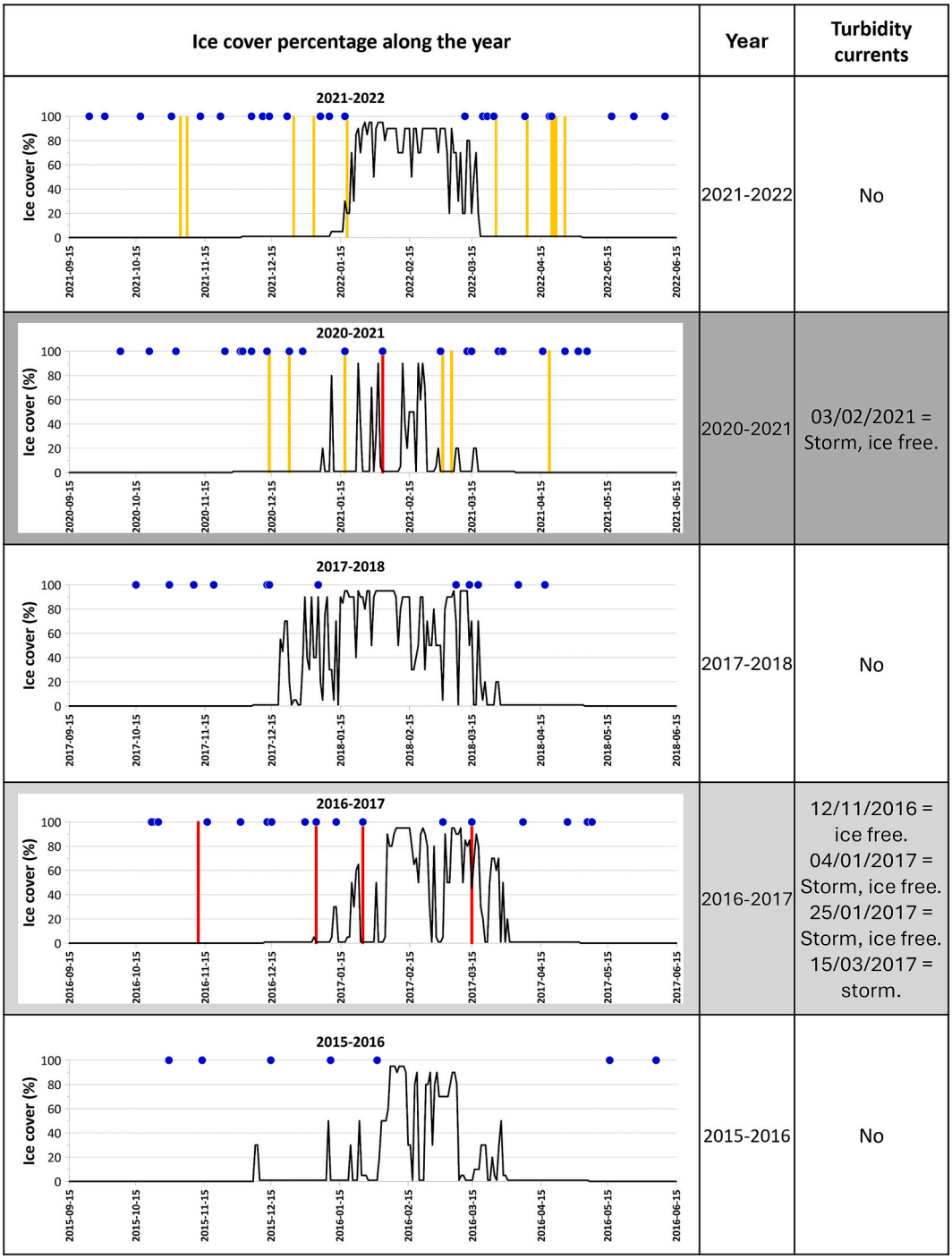

Fig. 12. Percentage of ice cover off PDM, major storms, and resuspension events in the canyon during five years. Blue dots represent storms with significant wave heights from observations at Saint-Ulric (60 km SSW) or Rivière-Pentecôte (50 km NNE). For 2020–2022, all storms that have generated wave heights above 2 m are presented (Neumeier and Joly, 2021, 2025). For 2015–2018, major storms are presented following Neumeier and Joly (2019, 2021). Vertical red bars indicate turbidity currents (for all years). Vertical yellow bars indicate the resuspension events shown in Fig. 3 and smaller events (only for 2020–2022). The period with no resuspension and almost no storms (June 6 to October 15) is not represented. (For interpretation of the references to colour in this figure legend, the reader is referred to the web version of this article.)

partial sediment winnowing. This change in hydrodynamics is consistent with the change in sediment activity observed in the bathymetry, where sediments become unconfined (Fig. 5D). Massive sand deposits in proximal cores likely result from hydraulic jumps generated by turbidity currents interacting with crescentic bedforms topography (Postma et al., 2009; Ghienne et al., 2021), leading to sediment mixing and complex depositional signatures.

Most turbidites in PDM are characterized by initial inverse grading followed by normal grading, as observed in cores COR2001-09BC and COR2212-04BC (Figs. 8 & 9). In particular, core COR2001-09BC displays two distinct inverse grading sequences composed of multiple laminae, followed by normal grading. Similar pulsed turbidity currents were recorded in 2017 (Normandeau et al., 2020) and 2021 (this study – ADCP data, Figs. 3A and 4), suggesting that such pulses may be responsible for the basal inverse grading. Alternatively, particle segregation at the base of the turbidity currents (Clare et al., 2016;

Normandeau et al., 2017) or flow convergence from multiple gullies at the canyon head may contribute to this pattern. This interpretation aligns with the findings of Heerema et al. (2022), who demonstrated that multiple pulses observed in both acoustic and sedimentary records can be triggered by various mechanisms, not solely by flood events.

Despite recent turbidity current activity documented through bathymetric and ADCP data, no typical turbidites are present at the top of the cores collected within the submarine fan. These cores contain at most two turbidity current deposits (Figs. 8G-I & 9) and ^{210}Pb-derived sedimentation rates of COR2212-05BC and COR2212-08BC (Figs. 10 & 11) indicate that these deposits predate any turbidity currents recorded during the multibeam or ADCP monitoring periods (i.e., COR2212-05BC, COR2001-10BC, COR2001-08BC, COR2212-08BC). Based on the observed recurrence of turbidity currents from Normandeau et al. (2014, 2020) and this study, a greater number of turbidity current deposits was expected in these distal cores, even if some flows were diluted and lacked dense basal layers. Their absence in cores suggests that the record of storm-induced turbidity currents over the last 15 years has not been preserved on the fan. These results highlight that sediment cores from the fan capture only a limited portion of canyon activity, despite the fan traditionally being a key area for reconstructing Quaternary canyon dynamics (e.g., Fauquembergue et al., 2019; Normandeau et al., 2023).

Older turbidites recorded in cores from the PDM fan may have been storm-induced, although other processes may have led to larger turbidity currents in the last centuries, leading to better preservation on the fan. PDM lies within the LSLE seismic zone (Lamontagne et al., 2003; Mazzotti et al., 2005), raising the possibility that the larger preserved turbidites could have been triggered by earthquakes (e.g., Mérindol et al., 2022). The ^{210}Pb chronology suggests that some remobilized turbidites, especially those in core COR2212-08BC, may correspond to known seismic events, such as the 1880 CE M ~ 5.5 earthquake at Pointe-aux-Anglais, located approximately 35 km northeast of PDM (Lamontagne et al., 2018; Fig. 1A). Earthquake-triggered channel-wall collapses could generate more powerful turbidity current capable of transporting greater sediment volumes to the fan. This contrasts with storm-induced turbidity current, which may be weaker due to limited sediment availability in the PDM system (rocky shoreline, small till-filled bay, and narrow sandy beach; Normandeau et al., 2014; Normandeau, 2015). Larger sediment volumes are also more likely to resist post-depositional reworking, for example by bottom currents, increasing the preservation potential of these deposits.

5.2.2. *Reworking of turbidites by bottom currents*

The lack of monitored turbidity current deposits in the sediment cores raises the question about the completeness and preservation of turbidite records. One key factor contributing to this gap is remobilization by bottom currents, which can occur throughout the year, either during or after deposition, resulting in bottom-reworked facies (Stanley, 1987; Figs. 7A-F & 8). In addition, bioturbation plays an important role in disrupting and erasing primary sedimentary structures (Figs. 7J-L & 8), further complicating the interpretation of recent sedimentary activity.

Nonetheless, features such as discontinuous sandy lenticules with angular or lateral boundaries, mud-offshoots, sigmoidal structures, and flaser bedding at the tops of certain turbidity current layers (Figs. 7 & 8) provide strong evidence for bottom-current remobilization in PDM cores (e.g., Shanmugam et al., 1993; Shanmugam, 2003; Rebesco et al., 2014; Rodrigues et al., 2022). Additional structures, such as deformed laminations, climbing ripples likely result from similar sedimentary processes. These sedimentary features may form during deposition, when bottom currents disrupt turbidity currents and entrain fine sediments (Miramontes et al., 2020; Rodrigues et al., 2022), or through post-depositional reworking.

In the proximal cores (COR2212-01BC, COR2001-13BC, COR2001-09BC, and COR2212-04BC), bioturbation appears very limited in the X-CT images, likely reflecting the more intense hydrodynamic conditions and recent deposition of turbidites. The combination of strong sedimentary and hydrodynamic forces, coupled with coarser sediment composition, creates an environment less favorable for benthic biological activity, which may explain the minimal bioturbation observed in these cores. The near absence of clay and finer particles suggests selective removal of the finer fraction, consistent with winnowing processes. This interpretation aligns with the observed sediment textures and supports the idea of active hydrodynamic conditions influencing sediment distribution in the distal parts of the system. Conversely, distal cores (COR2212-05BC, COR2001-10BC, COR2001-08BC, and COR2212-08BC) show frequent bioturbation (Fig. 7J-L), along with bottom-current remobilization structures at the top of turbidites and cores (Figs. 7A-F & 8). In cores COR2212-05BC, COR2001-10BC, and COR2212-08BC, most deposits exhibit remobilized normal grading, suggesting bottom-current influence on sedimentation. This reworking likely explains the poor preservation of typical turbidite structures. Interestingly, bottom-current structures are more widely observed in the distal area, a pattern that contrasts with finding from He et al. (2013), although on different time scales. In the Qiongdongnan Basin (northern South China Sea), they reported stronger bottom-current influence in the proximal part of the canyon. We attribute this discrepancy to differences in the frequency and magnitude of sediment-transport events and potentially to bottom-current strength. In the PDM canyon system, sediment input is limited, and storm-induced turbidity currents may lack a dense basal layer, while in the Qiongdongnan Basin, mass-transport deposits exert strong erosional and depositional effects in the distal area (He et al., 2013). Additional differences in regional oceanographic processes, canyon morphology and system scale likely also contribute to the different hydrodynamic responses.

The combined effect of bottom-current remobilization and bioturbation, as shown in the X-ray zoom images in Fig. 7, contribute to sediment mixing and complicate the preservation of turbidity current deposits. In addition, the presence of well-preserved organic/plant debris at the tops of cores COR2001-09BC (recovered in 2020) and COR2212-04BC (recovered in 2022), located close to each other (distance = 140 m), suggests that no significant sedimentation nor remobilization occurred between the two sampling periods in this area (Fig. 9) and that the turbidity current recorded by the mooring 02M on February 3, 2021, did not reach the submarine fans along the seafloor. Otherwise, a thin layer of sediment would likely have buried the organic/plant debris. Sharpe et al. (2023) associated this turbidity current with a peak in total particulate matter recorded in a nearby sediment trap, moored above core COR2212-05BC (Mooring 05M in Fig. 1). This particulate matter peak and the absence of turbidite on the seafloor suggests that the turbidity current lofted into the water column before reaching the fan and was likely entrained by bottom currents (similar to contour current reworking; Miramontes et al., 2020). In such cases, coarse particles settle rapidly while finer sediments propagate through the water column, leading to low sediment deposition and poor preservation of these events on the fan. Given the limited length and relief of the PDM canyon system, these results highlight the need for further investigation into the fate of dilute sediment plumes in larger systems.

Core site selection can also contribute to heterogeneity and the absence of recent turbidites (≤15 years) in the sediment cores. Submarine canyons are often dominated by erosional processes, and spatial variations in sediment flow paths can lead to heterogeneous sediment records within the same canyon system (e.g. He et al., 2013; Stacey et al., 2019; Sumner et al., 2012; Talling et al., 2012; Tang and Piper, 2020). However, the broad spatial distribution of cores in the PDM canyon system (particularly in the distal area), combined with the chronological framework of fan cores (COR2221-05BC and COR2212-08BC; Figs. 10 and Fig. 11, respectively) support the interpretation that post-depositional processes such as bottom currents and bioturbation significantly alter the sediment record (Figs. 7A-F & 8). These results underscore the importance of integrating sediment cores with

bathymetric and ADCP data to fully understand sedimentary processes in submarine canyon systems (e.g., de Castro et al., 2020; Normandeau et al., 2024; Stow and Smillie, 2020; Wolfson-Schwehr et al., 2023).

To date, the nature of the bottom currents in the PDM canyon system remains uncertain. Positioned between the LSLE and the Gulf of St. Lawrence, PDM is influenced by the interaction of multiple water masses and current systems, creating a complex hydrographic environment conducive to bottom-current activity (e.g., Tang, 1980; Koutitonsky et al., 1990; Cyr et al., 2015; Baccara, 2023). Bailey et al. (2024) reported that near-bed tidal currents in submarine canyons can be sufficiently strong to resuspend sediments, a mechanism likely active in the PDM canyon system given its hydrographic and oceanographic conditions. In addition, internal waves can drive sediment remobilization. Bourgault et al. (2014, 2007) and Boegman and Stastna (2019) demonstrated that internal waves interacting with the seafloor can resuspend sediments. Baccara (2023) observed such internal waves in the PDM water column during nearly every tidal cycle (Fig. 3H, I), although their activity was most active at shallower depths (120–180 m) than those sampled in most sediment cores. Similarly, modeling by Normandeau et al. (2014) suggests conditions favorable to strong bottom currents in the upper 120 m of the water column. However, the specifics of bottom currents at deeper depths (200–300 m), where sediment reworking is evident, remain poorly constrained. This knowledge gap highlights the need for future studies to better constrain the dynamics of these deeper currents and their role in shaping sedimentation patterns on the canyon floor.

Our data suggests that sediment cores from the PDM system reflect a complex depositional environment shaped by the interplay of multiple sedimentary processes (e.g., Campbell and Deptuck, 2012; de Castro et al., 2020; Miramontes et al., 2021). In such mixed systems, interactions among bottom currents, gravity flows, and bioturbation, can obscure or overprint individual sedimentary signals, complicating the interpretation of sediment core records. With no river flowing from the coast and overall low sediment supply, it is likely that bottom currents exert a relatively stronger influence on sediment distribution and facies development within the PDM system.

6. Conclusion

The PDM submarine canyons represent a sediment-starved system with relatively frequent turbidity currents, all of which have been linked to storm activity during ice-free conditions in the LSLE. Seafloor changes associated with turbidity currents are characterized primarily by the upslope migration of crescentic bedforms in proximal areas. Migration ceases or diminishes below the resolution of the dataset in the unconfined part of the system where turbidity currents spread, dilute, and lose energy.

Most of the short sediment cores (30–50 cm) collected across the PDM canyon system contain only two turbidite beds. All turbidites in the distal cores predate the nine turbidity currents recorded by the ADCP and repeat multibeam bathymetric data. Notably, none of the turbidity currents recorded between 2012 and 2022 were observed in the distal sediment cores according to the age model and sedimentation rates obtained. These results suggest that sediment cores in the PDM canyon system are not reliable archives of turbidity current activity. The absence of modern turbidity current deposits suggests that 1) the turbidity currents observed via ADCP data or bedform migration are not strong enough to deposit a significant sediment layer in the distal fan area and/or that 2) bottom currents remobilize turbidites during or after their deposition. While often underrecognized, bottom-current-reworked deposits play a significant role in shaping the sedimentary record of submarine canyons.

Given the large discrepancies in turbidity current deposit records observed across different techniques (multibeam bathymetric mapping, ADCP monitoring, and sediment core analysis), it is critical to use a combination of these methods for a comprehensive understanding of turbidity current processes in submarine canyons. Future efforts to assess turbidity current recurrence should focus on understanding the physical processes driving sediment deposition and remobilization, as this is key to interpreting sedimentary records and reconstructing the history of sedimentary systems. This integrated approach will improve our ability to document the recurrence of turbidity currents and enhance our understanding of mixed systems and of the long-term dynamics of submarine canyons.

CRediT authorship contribution statement

Florian Jacques: Writing – original draft, Visualization, Validation, Software, Resources, Methodology, Investigation, Funding acquisition, Formal analysis, Data curation, Conceptualization. **Alexandre Normandeau:** Writing – review & editing, Validation, Software, Resources, Funding acquisition, Conceptualization. **Jean-Carlos Montero-Serrano:** Writing – review & editing, Validation, Supervision, Resources, Project administration, Funding acquisition, Conceptualization. **Guillaume St-Onge:** Writing – review & editing, Validation, Supervision, Resources, Funding acquisition. **Audrey Limoges:** Writing – review & editing, Validation, Supervision, Resources, Project administration, Funding acquisition. **André Rochon:** Writing – review & editing, Validation, Supervision, Resources, Funding acquisition. **Urs Neumeier:** Writing – review & editing, Validation, Supervision, Resources, Funding acquisition, Software. **Patrick Lajeunesse:** Writing – review & editing, Resources. **Daniel Bourgault:** Writing – review & editing, Resources.

Declaration of competing interest

The authors declare that they have no known competing financial interests or personal relationships that could have appeared to influence the work reported in this paper.

Acknowledgments

We would like to thank the captain, officers, crew, and scientists onboard the R/V Coriolis II during the 2020, 2021, and 2022 RQM-MEOPAR expeditions for the acquisition of multibeam data and the recovery of the sediment samples used in this study. This study contributes to the research program *"Monitoring natural hazards during coastal to offshore sediment remobilization and its impacts on primary productivity dynamics in the Lower St. Lawrence Estuary"*, which is supported jointly by Réseau Québec maritime (RQM) and the Marine Environmental Observation Prediction and Response Network (MEOPAR). This study received further support from the Natural Sciences and Engineering Research Council of Canada (NSERC) through Discovery Grants to J.C. M.S., A.L., G.S., P.L., and A.R.; Geotop; Québec-Océan. We thank Odyssée Saint-Laurent (RQM) for Ship-Time grant. The acquisition of the wave data at Saint-Ulric and Rivière-Pentecôte was funded by the Government of Quebec (Ministère des Transports et de la Mobilité durable). We thank Geotop for the F.J. scholarship and the International Association of Sedimentologists (IAS) for the postgraduate research Grant (Fall 2023 Session) awarded to F.J. that allowed ^{210}Pb analysis. We also thank Christian Boutot (ISMER-UQAR), Sylvain Blondeau (Québec-Océan) and Natalie Pisciotto (CIDCO), who provided technical support during mooring recovery, CTD-rosette deployment, coring and geophysical operations; Pascal Rioux (ISMER-UQAR), who assisted with the preparation of the sampling material and transport logistics; Quentin Beauvais (ISMER-UQAR), who assisted with the physical property analyses; Claude Belzile (ISMER-UQAR), for the grain size analysis training, Dominique Lavallée (ISMER-UQAR), who assisted with the grain size analysis, Sylvain Joly (ISMER-UQAR) who processed the wave data, and Antonin Prijac (Geotop-UQAM), for ^{210}Pb analysis. We thank Jenna Higgins (GSC–Atlantic) for the laminography scans and help with the software used to visualize the laminography scans. Finally, we thank

Rebecca Englert (MBARI) and two anonymous reviewers for their constructive reviews, which significantly improved the quality of the manuscript. We also thank Michele Rebesco for his editorial support.

Appendix A. Supplementary data

Supplementary data to this article can be found online at https://doi.org/10.1016/j.margeo.2025.107660.

Data availability

All analytical data presented are available electronically in the Observatoire global du Saint-Laurent (https://doi.org/10.26071/7bb5f2d7-b91e-46ce).

References

Amundsen, H.B., Laberg, J.S., Vorren, T.O., Haflidason, H., Forwick, M., Buhl-Mortensen, P., 2015. Late Weichselian–Holocene evolution of the high-latitude Andøya submarine Canyon, North-Norwegian continental margin. Mar. Geol. 363, 1–14. ISSN 0025–3227. https://doi.org/10.1016/j.margeo.2015.02.002.

Azpiroz-Zabala, M., Cartigny, M.J., Talling, P.J., Parsons, D.R., Sumner, E.J., Clare, M.A., Simmons, S.M., Cooper, C., Pope, E.L., 2017. Newly recognized turbidity current structure can explain prolonged flushing of submarine canyons. Sci. Adv. 3 (10), e1700200. https://doi.org/10.1126/sciadv.1700200.

Baccara, K., 2023. Conditions océanographiques dans les canyons sous-marins de Pointe-des-Monts. MSc thesis. Rimouski, Université du Québec à Rimouski, Institut des sciences de la mer de Rimouski (ISMER), 80 p.

Bailey, L.P., Clare, M.A., Hunt, J.E., Kane, I.A., Miramontes, E., Fonnesu, M., Argiolas, R., Malgesini, G., Wallerand, R., 2024. Highly variable deep-sea currents over tidal and seasonal timescales. Nat. Geosci. 17, 787–794. https://doi.org/10.1038/s41561-024-01494-2.

Belzile, C., Montero-Serrano, J.-C., 2022. Quantifying simulated fine sand fraction in muddy sediment using laser diffraction. Can. J. Earth Sci. 59, 455–461. https://doi.org/10.1139/cjes-2022-0011.

Bigham, K.T., Rowden, A.A., Leduc, D., Bowden, D.A., 2021. Review and syntheses: impacts of turbidity flows on deep-sea benthic communities. Biogeosciences 18, 1893–1908. https://doi.org/10.5194/bg-18-1893-2021.

Blott, S.J., Pye, K., 2001. GRADISTAT: a grain size distribution and statistics package for the analysis of unconsolidated sediments. Earth Surf. Process. Landf. 26, 1237–1248. https://doi.org/10.1002/esp.261.

Boegman, L., Stastna, M., 2019. Sediment resuspension and transport by internal solitary waves. Annu. Rev. Fluid Mech. 51, 129–154. https://doi.org/10.1146/annurev-fluid-122316-045049.

Bourgault, D., Blokhina, M.D., Mirshak, R., Kelley, D.E., 2007. Evolution of a shoaling internal solitary wavetrain. Geophys. Res. Lett. 34, L03601. https://doi.org/10.1029/2006GL028462.

Bourgault, D., Morsilli, M., Richards, C., Neumeier, U., Kelley, D.E., 2014. Sediment resuspension and nepheloid layers induced by long internal solitary waves shoaling orthogonally on uniform slopes. Cont. Shelf Res. 72, 21–33. https://doi.org/10.1016/j.csr.2013.10.019.

Campbell, D.C., Deptuck, M.E., 2012. Alternating bottom-current-dominated and gravity flow-dominated deposition in a lower slope and rise setting—insights from the seismic geomorphology of the Western Scotian Margin, Eastern Canada. In: Prather, B.E., Deptuck, M.E., Mohrig, D., Van Hoorn, B., Wynn, R.B. (Eds.), Application of the Principles of Seismic Geomorphology to Continental-slope and Base-of-slope Systems: Case Studies from Seafloor and Near-seafloor Analogues, 99. SEPM Special Publication, pp. 329–346. https://doi.org/10.2110/pec.12.99.0329.

Clare, M.A., Hughes Clarke, J.E., Talling, P.J., Cartigny, M.J.B., Pratomo, D.G., 2016. Preconditioning and triggering of offshore slope failures and turbidity currents revealed by most detailed monitoring yet at a fjord-head delta. Earth Planet. Sci. Lett. 450, 208–220. https://doi.org/10.1016/j.epsl.2016.06.021.

Cyr, F., Bourgault, D., Galbraith, P.S., 2015. Behavior and mixing of a cold intermediate layer near a sloping boundary. Ocean Dyn. 65, 357–374. https://doi.org/10.1007/s10236-014-0799-1.

d'Anglejan, B., 1990. Recent sediments and sediment transport processes in the St. Lawrence Estuary. In: El-Sabh, M.I., Silverberg, N. (Eds.), Oceanography of a Large-Scale Estuarine System. Coastal and Estuarine Studies, vol. 39. Springer, New York, NY. https://doi.org/10.1007/978-1-4615-7534-4_6.

d'Anglejan, B.F., Smith, E.C., 1973. Distribution, transport, and composition of suspended matter in the St. Lawrence Estuary. Can. J. Earth Sci. 10, 1380–1396. https://doi.org/10.1139/e73-128.

de Vernal, A., St-Onge, G., Gilbert, D., 2011. Oceanography and Quaternary geology of the St. Lawrence Estuary and the Saguenay Fjord. IOP Conf. Ser. Earth Environ. Sci. 14, 012004. https://doi.org/10.1088/1755-1315/14/1/012004.

Dickie, L., Trites, R.W., 1983. The Gulf of St. Lawrence. In: Dickie, L., Trites, R.W. (Eds.), Estuaries and Semi-Enclosed Seas. Elsevier Scientific Publication, Amsterdam, The Netherlands, pp. 403–425.

Drinkwater, K.F., Gilbert, D., 2004. Hydrographic variability in the waters of the Gulf of St. Lawrence, the Scotian Shelf and the Eastern Gulf of Maine (NAFO Subarea 4) during 1991-2000. J. Northwest Atl. Fish. Sci. 34, 85–101. https://doi.org/10.2960/J.v34.m545.

El-Sabh, M.I., 1976. Surface circulation pattern in the Gulf of St. Lawrence. J. Fish. Res. Board Can. 33, 124–138. https://doi.org/10.1139/f76-015.

El-Sabh, M.I., Lie, H.-J., Koutitonsky, V.G., 1982. Variability of the near-surface residual current in the Lower St. Lawrence Estuary. J. Geophys. Res. 87 (CI2), 9589–9600. https://doi.org/10.1029/JC087iC12p09589.

Farquharson, W.I., 1966. St. Lawrence Estuary current surveys. In: Bedford Institute of Oceanography. Report 66–6, 84 pp.

Fauquembergue, K., Fournier, L., Zaragosi, S., Bassinot, F., Kissel, C., Malaizé, B., Caley, T., Moreno, E., Bachelery, P., 2019. Factors controlling frequency of turbidites in the Bengal fan during the last 248 kyr cal BP: clues from a presently inactive channel. Mar. Geol. 415, 105965. ISSN 0025-3227. https://doi.org/10.1016/j.margeo.2019.105965.

Fernandez-Arcaya, U., Ramirez-Llodra, E., Aguzzi, J., Allcock, A.L., Davies, J.S., Dissanayake, A., Harris, P., Howell, K., Huvenne, V.A.I., Macmillan-Lawler, M., Martín, J., Menot, L., Nizinski, M., Puig, P., Rowden, A.A., Sanchez, F., Van den Beld, I.M.J., 2017. Ecological role of submarine canyons and need for canyon conservation: a review. Front. Mar. Sci. 4, 5. https://doi.org/10.3389/fmars.2017.00005.

Forrester, W.D., 1974. Internal tides in the St. Lawrence Estuary. J. Mar. Res. 22, 55–66.

Gagné, H., Lajeunesse, P., St-Onge, G., Bolduc, A., 2009. Recent transfer of coastal sediments to the Laurentian Channel, Lower St. Lawrence Estuary (Eastern Canada), through submarine canyon and fan systems. Geo-Mar. Lett. 29, 191–200. https://doi.org/10.1007/s00367-009-0138-6.

Galbraith, P.S., 2006. Winter water masses in the Gulf of St. Lawrence. J. Geophys. Res. 111, C06022. https://doi.org/10.1029/2005JC003159.

Galbraith, P.S., Chassé, J., Dumas, J., Shaw, J.-L., Caverhill, C., Lefaivre, D., Lafleur, C., 2022. Physical Oceanographic Conditions in the Gulf of St. Lawrence during 2021. DFO Can. Sci. Advis. Sec. Res. Doc. 2022/034. iv + 83 p.

Galbraith, P.S., Chassé, J., Shaw, J.-L., Dumas, J., Lefaivre, D., Bourassa, M.-N., 2023. Physical oceanographic conditions in the Gulf of St. Lawrence during 2022. Can. Tech. Rep. Hydrogr. Ocean Sci. 354 : v + 88 p.

Galbraith, P.S., Sévigny, C., Bourgault, D., Dumont, D., 2024. Sea ice interannual variability and sensitivity to fall oceanic conditions and winter air temperature in the Gulf of St. Lawrence, Canada. J. Geophys. Res. Oceans 129, e2023JC020784. https://doi.org/10.1029/2023JC020784.

Ghaleb, B., 2009. Overview of the methods for the measurement and interpretation of short-lived radioisotopes and their limits. IOP Conf. Ser. Earth Environ. Sci. 5, 012007. https://doi.org/10.1088/1755-1307/5/1/012007.

Ghienne, J., Normandeau, A., Dietrich, P., Bouysson, M., Lajeunesse, P., Schuster, M., 2021. The depositional signature of cyclic steps: a late Quaternary analogue compared to modern active delta slopes. Sedimentology 68, 1502–1538. https://doi.org/10.1111/sed.12806.

Goldberg, E.D., 1963. Geochronology with 210 Pb in radioactive dating. Int. Atom. Energy Contrib. 1510, 121–131.

Government of Canada, 2024a. Historical Weather Data for Pointe-Des-Monts [Dataset]. Environment and Climate Change Canada. Retrieved April 13, 2024, from. https://climat.meteo.gc.ca/historical_data/search_historic_data_stations_f.html?searchType=stnName&timeframe=1&txtStationName=Pointe-des-Monts&searchMethod=contains&optLimit=yearRange&StartYear=2020&EndYear=2023&Year=2024&Month=4&Day=13&selRowPerPage=25.

Government of Canada, 2024b. Ice Archive, Gulf of St. Lawrence [Dataset]. Environment and Climate Change Canada. Retrieved February 5, 2025, from. https://iceweb1.cis.ec.gc.ca/Archive/page1.xhtml?lang=fr.

Hage, S., Cartigny, M.J.B., Clare, M.A., Sumner, E.J., Vendettuoli, D., Hughes Clarke, J.E., Hubbard, S.M., Talling, P.J., Lintern, D.G., Stacey, C.D., Englert, R.G., Vardy, M.E., Hunt, J.E., Yokokawa, M., Parsons, D.R., Hizzett, J.L., Azpiroz-Zabala, M., Vellinga, A.J., 2018. How to recognize crescentic bedforms formed by supercritical turbidity currents in the geologic record: insights from active submarine channels. Geology 46, 563–566. https://doi.org/10.1130/G40095.1.

He, Y., Xie, X., Kneller, B.C., Wang, Z., Li, X., 2013. Architecture and controlling factors of canyon fills on the shelf margin in the Qiongdongnan Basin, northern South China Sea. Mar. Pet. Geol. 41, 264–276. https://doi.org/10.1016/j.marpetgeo.2012.03.002.

Heerema, C.J., Cartigny, M.J.B., Jacinto, R.S., Simmons, S.M., Apprioual, R., Talling, P.J., 2022. How distinctive are flood-triggered turbidity currents? J. Sediment. Res. 92, 1–11. https://doi.org/10.2110/jsr.2020.168.

Heezen, B.C., Ewing, W.M., 1952. Turbidity currents and submarine slumps and the 1929 Grand Banks (Newfoundland) earthquake. Am. J. Sci. Ser. 250, 849–873.

Hubbard, S.M., Covault, J.A., Fildani, A., Romans, B.W., 2014. Sediment transfer and deposition in slope channels: deciphering the record of enigmatic deep-sea processes from outcrop. Geol. Soc. Am. Bull. 126, 857–871. https://doi.org/10.1130/B30996.

Hughes Clarke, J.E., 2016. First wide-angle view of channelized turbidity currents links migrating cyclic steps to flow characteristics. Nat. Commun. 7, 11896. https://doi.org/10.1038/ncomms11896.

Jaegle, M., 2015. Nature et origine des sédiments de surface de l'estuaire du Saint-Laurent. Thèse de M.Sc. Université du Québec à Rimouski, 83 pp.

Kostic, S., Parker, G., 2006. The response of turbidity currents to a canyon–fan transition: internal hydraulic jumps and depositional signatures. J. Hydraul. Res. 44, 631–653. https://doi.org/10.1080/00221686.2006.9521713.

Koutitonsky, V.G., Bugden, G.L., 1991. The physical oceanography of the Gulf of St. Lawrence: a review with emphasis on the synoptic variability of the motion. In: Therriault, J.-C. (Ed.), The Gulf of St. Lawrence: Small Ocean or Big Estuary? Can. Spec. Publ. Fish. Aquat. Sci, 113, pp. 57–90.

Koutitonsky, V.G., Wilson, R.E., El-Sabh, M.I., 1990. On the seasonal response of the Lower St Lawrence Estuary to buoyancy forcing by regulated river runoff. Estuar. Coast. Shelf Sci. 31, 359–379. https://doi.org/10.1016/0272-7714(90)90032-M.

Krishnaswamy, S., Lal, D., Martin, J.M., Meybeck, M., 1971. Geochronology of lake sediments. Earth Planet. Sci. Lett. 11, 407–414. https://doi.org/10.1016/0012-821X(71)90202-0.

Lamontagne, M., Keating, P., Perreault, S., 2003. Seismotectonic characteristics of the Lower St. Lawrence Seismic Zone, Quebec: insights from geology, magnetics, gravity, and seismics, 40, 20. https://doi.org/10.1139/e02-104.

Lamontagne, M., Halchuk, S.C., Cassidy, J.F., Rogers, G.C., 2018. Significant Canadian earthquakes 1600-2017. Commission géologique du Canada, Dossier public 8285, 37. https://doi.org/10.4095/311183.

Lavoie, D., Chassé, J., Simard, Y., Lambert, N., Galbraith, P.S., Roy, N., Brickman, D., 2016. Large-scale atmospheric and oceanic control on Krill transport into the St. Lawrence estuary evidenced with three-dimensional numerical modelling. Atmosphere-Ocean 54 (3), 299–325. https://doi.org/10.1080/07055900.2015.1082965.

Li, M.Z., Prescott, R.H., Robertson, A.G., 2019. Observation of internal tides and sediment transport processes at the head of Logan Canyon on central Scotian Slope, eastern Canada. J. Mar. Syst. 193, 103–125. https://doi.org/10.1016/j.jmarsys.2019.02.007.

Limoges, A., Normandeau, A., Lalande, C., Bernier, C., Montero-Serrano, J.-C., 2020. R/V Coriolis II expedition RQM-MEOPAR – COR2007 Coastal to offshore sediment remobilization and its impacts on primary production dynamics in the Lower St. Lawrence Estuary. Université du Québec à Rimouski (UQAR), Institut des sciences de la mer de Rimouski (ISMER), p. 28.

Lurton, X., 2010. An Introduction to Underwater Acoustics, 2nd edition. Springer, Berlin, pp. 24–26.

Martín-Chivelet, J., Fregenal Martínez, M.A., Chacón, B., 2008. Traction structures in contourites. In: Rebesco, M., Camerlenghi, A. (Eds.), Contourites. Developments in Sedimentology, 60. Elsevier, Amsterdam, pp. 159–181. https://doi.org/10.1016/S0070-4571(08)10010-3.

Mazzotti, S., James, T.S., Henton, J., Adams, J., 2005. GPS crustal strain, postglacial rebound, and seismic hazard in eastern North America: the Saint Lawrence valley example: crustal strain in Saint Lawrence valley. J. Geophys. Res. Solid Earth 110. https://doi.org/10.1029/2004JB003590.

McDonald, N., Bradwell, T., Callard, S.L., Toney, J.L., Shreeve, B., Shreeve, J., 2022. Automated characterisation of glaciomarine sediments using X-ray computed laminography. Quatern. Sci. Adv. 5. https://doi.org/10.1016/j.qsa.2021.100046.

McHargue, T., Pyrcz, M.J., Sullivan, M.D., Clark, J.D., Fildani, A., Romans, B.W., Covault, J.A., Levy, M., Posamentier, H.W., Drinkwater, N.J., 2011. Architecture of turbidite channel systems on the continental slope: patterns and predictions. Mar. Pet. Geol. 28, 728–743. https://doi.org/10.1016/j.marpetgeo.2010.07.008.

Meiburg, E., Kneller, B., 2010. Turbidity currents and their deposits. Annu. Rev. Fluid Mech. 42, 135–156. https://doi.org/10.1146/annurev-fluid-121108-145618.

Mérindol, M., St-Onge, G., Sultan, N., Lajeunesse, P., Garziglia, S., 2022. Submarine Landslides Triggered by the 1663 Earthquake (M>7) in the St. Lawrence Estuary, Quebec, Canada (other). display. https://doi.org/10.5194/egusphere-egu22-4835.

MINISTÈRE DES RESSOURCES NATURELLES ET DES FORÊTS, July 2023. Carte du relief à l'échelle de 1/2 000 000, [Data set], in Données Québec, 2019, updated 14. https://www.donneesquebec.ca/recherche/dataset/carte-du-relief-a-l-echelle-de-1-2-000-000 (accessed 11 July 2025).

Miramontes, E., Eggenhuisen, J.T., Poneti, G., Silva Jacinto, R., Pohl, F., Hernandez-Molina, F.J., 2020. Contour current-turbidity flow interaction from flume tank experiments: decoding processes and their morphological signatures. Geology 48, 353–357. https://doi.org/10.1130/G47111.1.

Miramontes, E., Thiéblemont, A., Babonneau, N., Penven, P., Raisson, F., Droz, L., Jorry, S., Fierens, R., Counts, J.W., Wilckens, H., Cattaneo, A., Jouet, G., 2021. Contourite and mixed turbidite-contourite systems in the Mozambique Channel (SW Indian Ocean): link between geometry, sediment characteristics and modelled bottom currents. Mar. Geol. 437, 106502. https://doi.org/10.1016/j.margeo.2021.106502.

Montero-Serrano, J.-C., Limoges, A., Normandeau, A., Corminboeuf, A., Laphengphratheng, T., 2020. R/V Coriolis II expedition RQM-MEOPAR – COR2001: Monitoring natural hazards during coastal to offshore sediment remobilization and its impacts on primary production dynamics in the Lower St. Lawrence Estuary. Université du Québec à Rimouski. Institut des sciences de la mer de Rimouski (ISMER), p. 54.

Neumeier, U., Joly, S., 2019. Stations d'observation des conditions maritimes 2014-2017 dans l'estuaire et le golfe du Saint-Laurent pour les problèmes d'érosion côtière. Rapport final présenté au ministère des Transports du Québec. Institut des sciences de la mer de Rimouski, Université du Québec à Rimouski xiv + 112 p.

Neumeier, U., Joly, S., 2021. Stations d'observation des conditions maritimes 2018-2021 dans l'estuaire et le golfe du Saint-Laurent pour les problèmes d'érosion côtière. Rapport final présenté au ministère des Transports du Québec. Institut des sciences de la mer de Rimouski, Université du Québec à Rimouski, 97 p.

Neumeier, U., Joly, S., 2025. Stations d'observation des conditions maritimes 2022-2024 dans l'estuaire et le golfe du Saint-Laurent et probabilités conjointes des vagues de tempêtes et des niveaux d'eau. Rapport final présenté au ministère des Transports du Québec. Institut des sciences de la mer de Rimouski, Université du Québec à Rimouski xxiii + 215 p.

Normandeau, A., 2015. Processus gravitaires tardi-quaternaires dans les canyons et chenaux sous-marins du Saint-Laurent (Est du Canada). PhD Thesis,. Université Laval.

Normandeau, A., Lajeunesse, P., St-Onge, G., Bourgault, D., Drouin, S.S.-O., Senneville, S., Bélanger, S., 2014. Morphodynamics in sediment-starved inner-shelf submarine canyons (Lower St. Lawrence Estuary, Eastern Canada). Mar. Geol. 357, 243–255. https://doi.org/10.1016/j.margeo.2014.08.012.

Normandeau, A., Lajeunesse, P., St-Onge, G., 2015. Submarine canyons and channels in the Lower St. Lawrence Estuary (Eastern Canada): morphology, classification and recent sediment dynamics. Geomorphology 241, 1–18. https://doi.org/10.1016/j.geomorph.2015.03.023.

Normandeau, A., Dietrich, P., Lajeunesse, P., St-Onge, G., Ghienne, J.-F., Duchesne, M.J., Francus, P., 2017. Timing and controls on the delivery of coarse sediment to deltas and submarine fans on a formerly glaciated coast and shelf. GSA Bull. 129 (11−12), 1424–1441. https://doi.org/10.1130/B31678.1.

Normandeau, A., Bourgault, D., Neumeier, U., Lajeunesse, P., St-Onge, G., Gostiaux, L., Chavanne, C., 2020. Storm-induced turbidity currents on a sediment-starved shelf: Insight from direct monitoring and repeat seabed mapping of upslope migrating bedforms. Sedimentology 67, 1045–1068. https://doi.org/10.1111/sed.12673.

Normandeau, A., Lajeunesse, P., Ghienne, J.-F., Dietrich, P., 2022. Detailed seafloor imagery of turbidity current bedforms reveals new insight into fine-scale near-bed processes. Geophys. Res. Lett. 49. https://doi.org/10.1029/2021GL097389 e2021GL097389.

Normandeau, A., Eamer, J., Bernatchez, P., Didier, D., Lajeunesse, P., Limoges, A., Montero-Serrano, J.-C., 2023. Sediment density flow distribution on wave-influenced deltas. Sedimentology 70, 100–120. https://doi.org/10.1111/sed.13033.

Normandeau, A., Dafoe, L.T., Li, M.Z., Campbell, D.C., Jenner, K.A., 2024. Sedimentary record of bottom currents and internal tides in a modern highstand submarine canyon head. Sedimentology 71, 1061–1083. https://doi.org/10.1111/sed.13165.

Paull, C.K., Talling, P.J., Maier, K.L., Parsons, D., Xu, J., Caress, D.W., Gwiazda, R., Lundsten, E.M., Anderson, K., Barry, Chaffey, M., O'Reilly, T., Rosemberger, K.J., Gales, J.A., Kieft, B., McGann, M., Simmons, S.M., McCann, M., Sumner, E.J., Clare, M.A., Cartigny, M.J., 2018. Powerful turbidity currents driven by dense basal layers. Nat. Commun. 9, 4114. https://doi.org/10.1038/s41467-018-06254-6.

Pinet, N., Brake, V., Campbell, C., 2011. Seafloor and shallow subsurface of the St. Lawrence River Estuary. Geosci. Can. 38, 10.

Piper, D.J.W., Normark, W.R., 2009. Processes that initiate turbidity currents and their influence on turbidites: a marine geology perspective. J. Sediment. Res. 79, 347–362. https://doi.org/10.2110/jsr.2009.046.

Pomar, L., Morsilli, M., Hallock, P., Bádenas, B., 2012. Internal waves, an under-explored source of turbulence events in the sedimentary record. Earth Sci. Rev. 111, 56–81. https://doi.org/10.1016/j.earscirev.2011.12.005.

Posamentier, H.W., Vail, P.R., 1988. Eustatic controls on clastic deposition II—Sequence and systems tract models. In: Wilgus, C.K., Hastings, B.S., Posamentier, H., Wagoner, J.V., Ross, C.A., St.C C.G., Kendall (Eds.), Sea-Level Changes: An Integrated Approach. SEPM Society for Sedimentary Geology, p. 0. https://doi.org/10.2110/pec.88.01.0125.

Postma, G., Cartigny, M.J.B., 2014. Supercritical and subcritical turbidity currents and their deposits–A synthesis. Geology 42, 987–990. https://doi.org/10.1130/G35957.1.

Postma, G., Cartigny, M.J.B., Kleverlaan, K., 2009. Structureless, coarse-tail graded Bouma Ta formed by internal hydraulic jump of the turbidity current? Sediment. Geol. 219, 1–6. https://doi.org/10.1016/j.sedgeo.2009.05.018.

Puig, P., Greenan, B.J.W., Li, M.Z., Prescott, R.H., Piper, D.J.W., 2013. Sediment transport processes at the head of Halibut Canyon, eastern Canada margin: an interplay between internal tides and dense shelf-water cascading. Mar. Geol. 341, 14–28. https://doi.org/10.1016/j.margeo.2013.05.004.

Puig, P., Palanques, A., Martín, J., 2014. Contemporary sediment-transport processes in submarine canyons. Annu. Rev. Mar. Sci. 6, 53–77. https://doi.org/10.1146/annurev-marine-010213-135037.

Rebesco, M., Hernandez-Molina, F.J., van Rooij, D., Wahlin, A., 2014. Contourites and associated sediments controlled by deep-water circulation processes: state-of-theart and future considerations. Mar. Geol. 352, 111–154. https://doi.org/10.1016/j.margeo.2014.03.011.

Rodrigues, S., Hernández-Molina, F.J., Fonnesu, M., Miramontes, E., Rebesco, M., Campbell, D.C., 2022. A new classification system for mixed (turbidite-contourite) depositional systems: examples, conceptual models and diagnostic criteria for modern and ancient records. Earth Sci. Rev. 230, 104030. https://doi.org/10.1016/j.earscirev.2022.104030.

Saucier, F.J., Chassé, J., 2000. Tidal circulation and buoyancy effects in the St. Lawrence Estuary. Atmosphere-Ocean 38, 505–556. https://doi.org/10.1080/07055900.2000.9649658.

Saucier, F.J., Roy, F., Gilbert, D., Pellerin, P., Ritchie, H., 2003. Modeling the formation and circulation processes of water masses and sea ice in the Gulf of St. Lawrence, Canada. J. Geophys. Res. Oceans 108, 3269. https://doi.org/10.1029/2000JC000686.

Shanmugam, G., 2003. Deep-marine tidal bottom currents and their reworked sands in modern and ancient submarine canyons. Mar. Pet. Geol. 20, 471–491. https://doi.org/10.1016/S0264-8172(03)00063-1.

Shanmugam, G., 2008. Deep-water bottom currents and their deposits. In: Rebesco, M., Camerlenghi, A. (Eds.), Contourites, Developments in Sedimentology, 60. Elsevier, Amsterdam, pp. 59–81. https://doi.org/10.1016/S0070-4571(08)10005-X.

Shanmugam, G., Spalding, T.D., Rofheart, D.H., 1993. Traction structures in deep-marine bottom-current reworked sands in the Pliocene and Pleistocene, Gulf of Mexico. Geology 21, 929–932. https://doi.org/10.1130/0091-7613(1993)021%3C0929:TSIDMB%3E2.3.CO;2.

Sharpe, H., Gosselin, M., Lalande, C., Normandeau, A., Montero-Serrano, J.-C., Baccara, K., Bourgault, D., Sherwood, O., Limoges, A., 2023. Influence of a small submarine canyon on biogenic matter export flux in the Lower St. Lawrence Estuary, eastern Canada. https://doi.org/10.5194/egusphere-2023-1538.

Sheng, J., 2001. Dynamics of a buoyancy-driven coastal jet: the Gaspé current. J. Phys. Oceanogr. 31 (11), 3146–3162. https://doi.org/10.1175/1520-0485(2001)031<3146:DOABDC>2.0.CO;2.

Shepard, F.P., 1981. Submarine canyons: multiple causes and long-time persistence. AAPG Bull. 65. https://doi.org/10.1306/03B59459-16D1-11D7-8645000102C1865D.

Shepard, F.P., Marshall, N.F., 1973. Currents along floors of submarine canyons. AAPG Bull. 57, 244–264. https://doi.org/10.1306/819A4266-16C5-11D7-8645000102C1865D.

Smith, J.N., Schafer, C.T., 1999. Sedimentation, bioturbation, and Hg uptake in the sediments of the estuary and Gulf of St. Lawrence. Limnol. Oceanogr. 44, 207–219. https://doi.org/10.4319/lo.1999.44.1.0207.

Squire, V.A., 2020. Ocean wave interactions with sea ice: a reappraisal. Annu. Rev. Fluid Mech. 52, 37–60. https://doi.org/10.1146/annurev-fluid-010719-060301.

Stacey, C.D., Hill, P.R., Talling, P.J., Enkin, R.J., Hughes Clarke, J., Lintern, D.G., 2019. How turbidity current frequency and character varies down a fjord-delta system: combining direct monitoring, deposits and seismic data. Sedimentology 66, 1–31. https://doi.org/10.1111/sed.12488.

Stanley, D.J., 1987. Turbidite to current-reworked sand continuum in upper cretaceous rocks. U.S. Virgin Islands Mar. Geol. 78, 143–151. https://doi.org/10.1016/0025-3227(87)90073-9.

St-Onge, G., Mulder, T., Francus, P., Long, B., 2007. Chapter two continuous physical properties of cored marine sediments. In: Developments in Marine Geology. Elsevier, pp. 63–98. https://doi.org/10.1016/S1572-5480(07)01007-X.

St-Onge, G., Duchesne, M.J., Lajeunesse, P., 2011. Marine geology of the St. Lawrence Estuary. IOP Conf. Ser. Earth Environ. Sci. 14, 012003. https://doi.org/10.1088/1755-1315/14/1/012003.

Stow, D.A.V., Faugères, J.C., 2008. Contourite facies and the facies model. In: Rebesco, M., Camerlenghi, A. (Eds.), Contourites. Developments in Sedimentology, 60. Elsevier, Amsterdam, pp. 223–256. https://doi.org/10.1016/S0070-4571(08)10013-9.

Stow, D., Smillie, Z., 2020. Distinguishing between deep-water sediment facies: turbidites, Contourites and Hemipelagites. Geosciences 10 (2), 68. https://doi.org/10.3390/geosciences10020068.

Sumner, E.J., Talling, P.J., Amy, L.A., Wynn, R.B., Stevenson, C., Frenz, M., 2012. Facies architecture of individual basin-plain turbidites: comparison to existing models and implications for flow processes. Sedimentology. https://doi.org/10.1111/j.1365-3091.2012.01329.x.

Talling, P.J., Sumner, E.J., Masson, D.G., Malgesini, G., 2012. Subaqueous sediment density flows: depositional processes and deposit types. Sedimentology 59, 1937–2003. https://doi.org/10.1111/j.1365-3091.2012.01353.x.

Talling, M.J., Cartigny, P.J., Pope, E., Baker, M., Clare, M.A., Heijnen, M., Hage, S., Parsons, D.R., Simmons, S.M., Paull, C.K., Gwiazda, R., Lintern, G., Hughes Clarke, J. E., Xu, J., Jacinto, R.S., Maier, K.L., 2023. Detailed monitoring reveals the nature of submarine turbidity currents. Nat. Rev. Earth Environ. 4 (9), 642–658. https://doi.org/10.1038/s43017-023-00458-1.

Tang, C.L., 1980. Mixing and circulation in the northwestern Gulf of St. Lawrence: a study of a buoyancy-driven current system. J. Geophys. Res. 85, 2787. https://doi.org/10.1029/JC085iC05p02787.

Tang, M., Piper, D.J.W., 2020. Down-canyon evolution of turbidity currents at a late-glacial ice margin: Halibut Canyon, offshore southeastern Canada. Mar. Geol. 424, 106182. https://doi.org/10.1016/j.margeo.2020.106182.

Viana, A.R., Faugères, J.-C., Stow, D.A.V., 1998. Bottom current controlled sand deposits – a review of modern shallow- to deep-water environments. Sediment. Geol. 115, 53–80. https://doi.org/10.1016/S0037-0738(97)00087-0.

Wells, M.G., Dorrell, R.M., 2021. Turbulence processes within turbidity currents. Annu. Rev. Fluid Mech. 53, 59–83. https://doi.org/10.1146/annurev-fluid-010719-060309.

Wolfson-Schwehr, M., Paull, C.K., Caress, D.W., Gwiazda, R., Nieminski, N.M., Talling, P. J., et al., 2023. Time-lapse Seafloor surveys reveal how turbidity currents and internal tides in Monterey Canyon interact with the seabed at centimeter-scale. J. Geophys. Res. Earth 128, e2022JF006705. https://doi.org/10.1029/2022JF006705.

Xu, J.P., Barry, J.P., Paull, C.K., 2013. Small-scale turbidity currents in a big submarine canyon. Geology 41 (2), 143–146. https://doi.org/10.1130/G33727.1.